Title
Multidimenstional Models for Macroscopic Virus Transport in Porous Media

Authors
Chrysikopoulos, Constantinos V
Sim, Youn

Publication Date
1997-07-01

Multidimensional Models for Macroscopic Virus Transport in Porous Media

BY

CONSTANTINOS V. CHRYSIKOPOULOS AND YOUN SIM

Department of Civil and Environmental Engineering
University of California, Irvine, CA 92697-2175

TECHNICAL COMPLETION REPORT

Project Number UCAL-WRC-W-854

July, 1997

University of California Water Resources Center

ABSTRACT

Analytical models for virus transport in saturated, homogeneous porous media are developed. The models account for three–dimensional dispersion in a uniform flow field, and first–order inactivation of suspended and deposited viruses with different inactivation rate coefficients. Virus deposition onto solid particles is described by two different processes: nonequilibrium adsorption which is applicable to viruses behaving as solutes; and colloid filtration which is applicable to viruses behaving as colloids. The governing virus transport equations are solved analytically by employing Laplace, Fourier, and finite Fourier cosine transform techniques. Instantaneous and continuous/periodic virus loadings from either a point or an elliptic source geometry are examined. Furthermore, porous media with either infinite, semi–infinite, or finite thickness are considered. The effects of virus loading conditions, aquifer boundary conditions, and virus source geometry on virus migration in subsurface porous formations are investigated.

A model for virus transport in one–dimensional, homogeneous, saturated porous media is also developed, accounting for virus sorption and inactivation of liquid phase and adsorbed viruses with different time dependent rate coefficients. The virus inactivation process is represented by a pseudo first–order rate expression. The pseudo first–order approximation is shown to simulate available experimental data from three virus inactivation batch studies better than the frequently employed constant rate inactivation model. Model simulations indicated that the pseudo first–order approximation, compared to the constant inactivation, leads to extended survival of viruses, and consequently more distant migration. Results from a parameter sensitivity analysis demonstrated that estimation of pseudo first–order inactivation rate coefficients from field observations requires data collection near the source of virus contamination during initial stages of virus transport.

KEY WORDS: virus transport, analytical/numerical modeling, multidimensional systems, non–equilibrium adsorption, filtration, time dependent virus inactivation.

TABLE OF CONTENTS

List of Tables

LIST OF FIGURES

a	semi–axis of the elliptic source parallel to x–axis, L
a_1, a_2	defined in (33) and (34), respectively
$\mathcal{A}$	defined in (5)
b	semi–axis of the elliptic source parallel to y–axis, L
$\mathcal{B}$	defined in (6)
C	concentration of virus in suspension (liquid phase), M/L^3
C_o	source concentration, M/L^3
C^*	deposited (or filtered) virus concentration (virus mass/solids mass), M/M
C_g	concentration of virus directly in contact with solids, M/L^3
C_∞	steady state virus concentration, M/L^3
d, d_1, d_2	defined in (A48), (A49), and (A50), respectively
D_x	longitudinal hydrodynamic dispersion coefficient, L^2/t
D_y	lateral hydrodynamic dispersion coefficient, L^2/t
D_z	vertical hydrodynamic dispersion coefficient, L^2/t
$\mathrm{erf}[x]$	error function, equal to $(2/\pi^{1/2}) \int_0^x e^{-z^2} dz$.
E	defined in (A7)
$\mathcal{E}$	defined in (C2)
f	defined in (A22)
f_o, f_1, f_2, f_3	arbitrary functions
F	general functional form of virus source configuration, M/L^3t
$\mathcal{F}^{-1}$	Fourier inverse operator
$\mathcal{F}_{\mathrm{fc}}$	finite Fourier cosine transform operator
$\mathcal{F}_{\mathrm{fc}}^{-1}$	finite Fourier cosine inverse operator
g	defined in (A30)
g_o	defined in (C12)
G	virus source loading function, M/t
h, h_1, h_2	defined in (A39), (A40) and (A41), respectively
H	finite aquifer thickness, L
$\mathcal{H}$	defined in (7)
$I_o[\ ]$	modified Bessel function of first kind of order zero
$I_1[\ ]$	modified Bessel function of first kind of first order
$J_o[\ ]$	Bessel function of first kind of order zero
k	mass transfer rate constant, t^{-1}
k_c	clogging rate constant, t^{-1}
k_r	declogging rate constant, t^{-1}
K_d	partition or distribution coefficient, L^3M^{-1}
$K_o[\ ]$	modified Bessel function of second kind of order zero
$\ell_{x_o}, \ell_{y_o}, \ell_{z_o}$	x, y and z Cartesian coordinates, respectively, of the virus point source, L
$\mathcal{L}$	Laplace transform operator

$\mathcal{L}^{-1}$	Laplace inverse operator
m	integer summation index
M	total virus mass released into the porous formation, M
$\mathcal{M}$	defined in (B2)
$\mathcal{M}_1, \mathcal{M}_2, \mathcal{M}_3$	defined in (C14), (C15), and (C16), respectively
n	wave number
$\mathcal{N}, \mathcal{N}_1, \mathcal{N}_2$	defined in (A32), (A33), and (A34), respectively
p	dummy integration variable
$\mathcal{P}$	defined in (A52)
PFU	plaque–forming units, M
$\mathcal{P}_1$	defined in (B25)
q	dummy integration variable
Q	defined in (13)
$\mathcal{Q}$	defined in (B16)
r	radius of circular source, L
r_1	forward rate coefficient, t^{-1}
r_2	reverse rate coefficient, M/L^3t
s	Laplace transform variable with respect to time
$\mathcal{S}$	defined in (A23)
$\mathcal{S}_1$	defined in (C8)
sse	sum of squared error.
t	time, t
t_o	arbitrary time, t
t_p	temporal period, t
U	average interstitial velocity, L/t
v	dummy integration variable
W	virus source geometry function, L^{-3}
x, y, z	spatial coordinates, L
Z	sensitivity coefficient for liquid phase concentration.
Z^*	sensitivity coefficient for adsorbed concentration.

Greek Letters

α	resistivity coefficient of liquid phase virus inactivation, t^{-1}.
α^*	resistivity coefficient of adsorbed virus inactivation, t^{-1}.
$\alpha_1, \alpha_2, \alpha_3$	arbitrary constants
$\beta, \beta_1, \beta_2, \beta_3$	arbitrary constants
γ	Fourier transform variable with respect to spatial coordinate x
$\delta(\ )$	Dirac delta function
ζ	dummy integration variable
η	defined in (B19)
θ	porosity (liquid volume/porous medium volume), L^3/L^3
Θ	defined in (C10)
$\kappa, \kappa_1, \kappa_2$	defined in (37a), (35), and (36), respectively
λ	inactivation rate coefficient of liquid phase viruses, t^{-1}
λ_o	initial inactivation rate coefficient of liquid phase viruses, t^{-1}.
λ^*	inactivation rate coefficient of deposited viruses, t^{-1}

λ_o^*	initial inactivation rate coefficient of adsorbed viruses, t^{-1}.
$\Lambda_1, ..., \Lambda_7$	defined in (21a), (21b), (21c), (28a), (28b), (32), and (41), respectively
μ	arbitrary argument
ξ	dummy integration variable
ρ	bulk density of the solid matrix (solids mass/aquifer volume), M/L^3
τ	dummy integration variable
ϕ	Fourier or Laplace transform variable with respect to spatial coordinate z in Appendix A or Appendix B & C, respectively
Φ	defined in (A25)
Φ_1	defined in (B9)
ψ_m	finite Fourier cosine transform variable with respect to spatial coordinate z, defined in (42)
Ψ	defined in (A19)
Ψ_1	defined in (C7)
ω	Fourier transform variable with respect to spatial coordinate y
Ω_n	spectrum of known coefficients, M/t
$\overline{\Omega}$	mean virus mass release rate, M/t

Groundwater contamination by pathogens such as viruses and bacteria is a serious public health concern. An increasing number of disease outbreaks associated with viral contamination of groundwater has been observed in the recent years (Matthess et al., 1988; Yahya et al., 1993; Gupta and Chaudhuri, 1995). It should be noted that even very low numbers of viruses in groundwater may cause a serious health hazard (Bitton and Gerba, 1984; Huber et al., 1994). Therefore, a complete understanding of the fate and transport of viruses in subsurface formations is crucial. Typical sources of viral contamination of groundwater are land disposal of sewage sludge and effluents, groundwater recharge with reclaimed water, breakage or spillage of onsite sewage disposal units (e.g., septic tanks and cesspools), and land disposal of solid wastes (e.g., sanitary landfills).

Mathematical models of virus transport in porous formations can effectively be utilized in determining the optimal location of wastewater or sludge disposal, in order to minimize possible impact on groundwater quality of nearby drinking water wells (Yates and Ouyang, 1992). However, there are only a few one–dimensional analytical (i.e., Vilker et al., 1978; Sim and Chrysikopoulos, 1995; Chrysikopoulos and Sim, 1996) and numerical (i.e., Grosser, 1984; Haridas, 1984; Tim and Mostaghimi, 1991; Park *et al.*, 1992; Yates and Ouyang, 1992; Sim and Chrysikopoulos, 1996) models available in the literature for the prediction of fate and transport of viruses in subsurface formations. Furthermore, although several multidimensional analytical models for solute transport are available in the literature (i.e., Hunt, 1978; Goltz and Roberts, 1986; van Dujin and van der Zee, 1986; Batu, 1989, 1993; Batu and van Genuchten, 1990; Leij and Dane, 1990; Leij *et al.*, 1991, 1993; Bellin *et al.*, 1993; Chrysikopoulos *et al.*, 1994; Chrysikopoulos, 1995; van Kooten, 1996), multidimensional analytical models describing virus fate and transport in subsurface porous media are nonexisting.

Viruses are submicron particles containing nucleic acids, either RNA or DNA, in a protein coat called capsid. Viruses may lose their infectivity due to disruption of coat proteins and degradation of nucleic acid (Gerba, 1984). This process is known as inactivation. In subsurface formations, inactivation is controlled mainly by the physicochemical characteristics of viruses (e.g., size, chemical composition, protein coat packaging) (Yamagishi and Ozeki, 1972), and external factors associated with geochemical heterogeneities of the porous medium (e.g., formation properties, temperature variations) (Yates and Yates, 1988). Therefore, the relatively complex nature of subsurface formations may lead to spatially as well as temporally variable virus inactivation.

Temporal variation of inactivation rate coefficients due to variabilities of virus characteristics has been observed in several experimental studies. Parkinson and Huskey (1971) and Pollard and Solosko (1971) noticed that *bacteriophage–*λ and T_4 populations consist of two subpopulations with different resistance to heat (biphasic inactivation). They observed that the most sensitive viruses inactivate rapidly, while the remaining more resistant viruses undergo slower inactivation. Similarly, Yamagishi and Ozeki (1972) reported that the inactivation of *bacteriophage–*λ exhibits two or more distinct phases (multiphasic inactivation), corresponding to subpopulations undergoing sequential inactivation with different inactivation rate coefficients. Grant et al. (1993) also observed multiphasic sequential inactivation of *bacteriophage–*λ during batch experiments with and without the presence of sand.

Traditionally, models for virus transport through porous formations assume that the inactivation rate coefficients are constant (Yates and Ouyang, 1992; Chrysikopoulos and Sim, 1996). It should be noted, however, that sequential inactivation of a virus population requires two or more discrete first–order rate coefficients, each governing a different inactivation phase (Crane and Moore, 1986). For mathematical simplicity,

the multiphasic sequential inactivation can be approximated by a pseudo first–order expression with a time dependent inactivation rate coefficient.

The present study focuses on the development of analytical solutions to multidimensional virus transport models. A variety of virus source configurations including continuous as well as periodic virus loadings from either point or elliptic source geometries are considered. Generalized analytical solutions applicable to viruses undergoing nonequilibrium adsorption or filtration in aquifers of semi–infinite as well as finite thickness are derived. Furthermore, the present work introduces a model for one–dimensional virus transport in homogeneous, saturated porous media accounting for virus sorption and inactivation with time dependent rate coefficients. The inactivation process is represented by a pseudo first–order expression with time dependent rate coefficients determined from available experimental data. Model simulations are compared to the frequently considered case of constant inactivation rate coefficients. In addition, sensitivity analysis is conducted to evaluate the response of the virus transport model to inactivation rate fluctuations.

The transport of viruses in saturated, homogeneous porous media, accounting for three–dimensional hydrodynamic dispersion in a uniform flow field, virus adsorption (or filtration), and first–order inactivation of liquid phase and deposited viruses with different inactivation rate coefficients, is governed by the following partial differential equation

$$\frac{\partial C(t,x,y,z)}{\partial t}+\frac{\rho}{\theta}\frac{\partial C^*(t,x,y,z)}{\partial t}-D_x\frac{\partial^2 C(t,x,y,z)}{\partial x^2}-D_y\frac{\partial^2 C(t,x,y,z)}{\partial y^2}$$
$$-D_z\frac{\partial^2 C(t,x,y,z)}{\partial z^2}+U\frac{\partial C(t,x,y,z)}{\partial x}+\lambda C(t,x,y,z)+\lambda^*\frac{\rho}{\theta}C^*(t,x,y,z)$$
$$=F(t,x,y,z), \tag{1}$$

where C is the liquid phase virus concentration; C^* is the virus concentration deposited onto the solid matrix; D_x, D_y, and D_z are the longitudinal, lateral, and vertical hydrodynamic dispersion coefficients, respectively; U is the average interstitial velocity; t is time; x, y, and z are the spatial coordinates in the longitudinal, lateral, and vertical directions, respectively; ρ is the bulk density of the solid matrix; θ is the porosity of the porous medium; λ is the inactivation rate coefficient of liquid phase viruses; λ^* is the inactivation rate coefficient of deposited viruses; and F is a general form of the virus source configuration. The accumulation of deposited viruses onto the solid matrix is described by the following generalized mass balance expression

$$\frac{\rho}{\theta}\frac{\partial C^*(t,x,y,z)}{\partial t}=r_1C(t,x,y,z)-r_2C^*(t,x,y,z)-\lambda^*\frac{\rho}{\theta}C^*(t,x,y,z), \tag{2}$$

where r_1 and r_2 are the forward and the reverse rate coefficients.

Assuming that initially there are no deposited viruses present in the porous formation, the expression describing C^* is obtained by solving (2) subject to the initial condition $C^*(0,x,y,z)=0$ to yield

$$C^*(t,x,y,z)=\frac{r_1\theta}{\rho}\int_0^t C(\tau,x,y,z)\exp\left[-\left(\frac{r_2\theta}{\rho}+\lambda^*\right)(t-\tau)\right]d\tau, \tag{3}$$

where τ is a dummy integration variable. In view of (2) and (3) the governing equation (1) can be written as

$$\frac{\partial C(t,x,y,z)}{\partial t} - D_x\frac{\partial^2 C(t,x,y,z)}{\partial x^2} - D_y\frac{\partial^2 C(t,x,y,z)}{\partial y^2} - D_z\frac{\partial^2 C(t,x,y,z)}{\partial z^2}$$

$$+ U\frac{\partial C(t,x,y,z)}{\partial x} + \mathcal{A}C(t,x,y,z) - \mathcal{B}\int_0^t C(\tau,x,y,z)e^{-\mathcal{H}(t-\tau)}d\tau = F(t,x,y,z), \quad (4)$$

where the following substitutions have been employed

$$\mathcal{A} = r_1 + \lambda, \quad (5)$$

$$\mathcal{B} = \frac{r_1 r_2 \theta}{\rho}, \quad (6)$$

$$\mathcal{H} = \frac{r_2\theta}{\rho} + \lambda^*. \quad (7)$$

The derived integrodifferential equation (4) is solved analytically in the subsequent sections for the cases of aquifers with infinite, semi–infinite, and finite thickness.

Aquifer with Infinite Thickness

The appropriate initial and boundary conditions for the case of an aquifer with infinite longitudinal, lateral, and vertical directions, as illustrated schematically in Figure 1a, are as follows

$$C(0,x,y,z) = C^*(0,x,y,z) = 0, \quad (8)$$

$$C(t,\pm\infty,y,z) = 0, \quad (9)$$

$$C(t,x,\pm\infty,z) = 0, \quad (10)$$

$$C(t,x,y,\pm\infty) = 0. \quad (11)$$

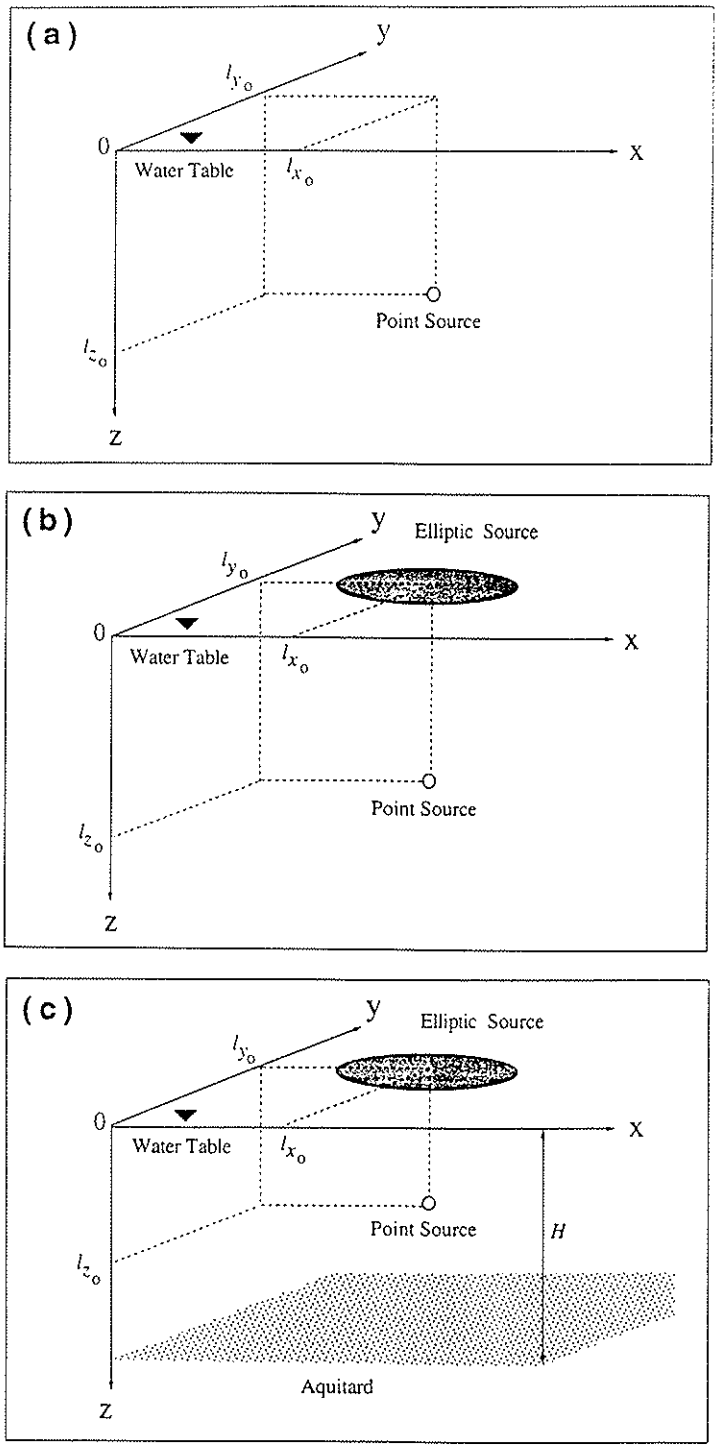

Figure 1: Schematic illustaration of point and elliptic sources of virus contamination with coordinates ℓ_{x_o}, ℓ_{y_o}, ℓ_{z_o} in an aquifer with (a) infinite, (b) semi–infinite, and (c) finite thickness. Note that the positive direction for the vertical coordinate is inverted.

Equation (4) subject to conditions (8)–(11) is solved analytically by straightforward but laborious procedures. Taking Laplace transforms with respect to time variable t and Fourier transforms with respect to space variables x, y, and z of (4) and subsequently employing the transformed initial and boundary conditions, followed by inverse transformations yields the desired analytical solution (see Appendix A)

$$C(t,x,y,z) = \left(\frac{1}{16\pi^2 D_x D_y}\right)^{1/2} \int_0^t \int_{-\infty}^{\infty} \int_{-\infty}^{\infty} \int_{-\infty}^{\infty} \exp\left[\frac{U(x-q)}{2D_x}\right] F(t-\tau,q,v,p)$$
$$\times \left[\mathcal{H}Q(\tau,x-q,y-v,z-p) + \frac{\partial Q(\tau,x-q,y-v,z-p)}{\partial \tau}\right] dp\, dv\, dq\, d\tau, \quad (12)$$

where

$$Q(t,x,y,z) = e^{-\mathcal{H}t} \int_0^t I_\circ\left[2\left(\mathcal{B}\zeta(t-\zeta)\right)^{1/2}\right] \left(\frac{1}{4\pi D_z \zeta^3}\right)^{1/2}$$
$$\times \exp\left[-\frac{1}{4\zeta}\left(\frac{x^2}{D_x} + \frac{y^2}{D_y} + \frac{z^2}{D_z}\right) - \zeta\left(\mathcal{A} + \frac{U^2}{4D_x} - \mathcal{H}\right)\right] d\zeta, \quad (13)$$

$$\frac{\partial Q(t,x,y,z)}{\partial t} = e^{-\mathcal{H}t} \int_0^t \left\{\left(\frac{\mathcal{B}\zeta}{t-\zeta}\right)^{1/2} I_1\left[2\left(\mathcal{B}\zeta(t-\zeta)\right)^{1/2}\right] - \mathcal{H} I_\circ\left[2\left(\mathcal{B}\zeta(t-\zeta)\right)^{1/2}\right]\right\}$$
$$\times \left(\frac{1}{4\pi D_z \zeta^3}\right)^{1/2} \exp\left[-\frac{1}{4\zeta}\left(\frac{x^2}{D_x} + \frac{y^2}{D_y} + \frac{z^2}{D_z}\right) - \zeta\left(\mathcal{A} + \frac{U^2}{4D_x} - \mathcal{H}\right)\right] d\zeta$$
$$+ e^{-\mathcal{H}t} \left(\frac{1}{4\pi D_z t^3}\right)^{1/2} \exp\left[-\frac{1}{4t}\left(\frac{x^2}{D_x} + \frac{y^2}{D_y} + \frac{z^2}{D_z}\right) - t\left(\mathcal{A} + \frac{U^2}{4D_x} - \mathcal{H}\right)\right], \quad (14)$$

p, q, v, and ζ are dummy integration variables, and $I_\circ$ and I_1 are the modified Bessel functions of the first kind of zeroth and first order, respectively. It should be noted that the Leibnitz rule (Greenberg, 1978, eq. 1.41, p. 18) as well as the Bessel function relationships $dI_\circ[\mu]/d\mu = I_1[\mu]$ (Abramowitz and Stegun, 1972, eq. 9.6.27, p. 376) and $I_\circ[0] = 1$ were employed in the derivation of (14).

Virus Source Configuration

The virus source configuration is represented by the following general function

$$F(t,x,y,z) = G(t)W(x,y,z), \tag{15}$$

where $G(t)$ is the virus mass release rate from the source; and $W(x,y,z)$ signifies the inverse of the source volume from which the virus mass is introduced into a porous medium. It should be noted, however, that $G(t)$ characterizes the source loading type. In the inifinite thickness aquifer case, instantaneous as well as continuous or temporally periodic source loading functions are considered.

Point Source Geometry

The point source geometry can be applied to represent virus sources such as broken sewer pipelines, leaking septic tanks, and groundwater recharge by injection wells, as described mathematically by the following expression

$$W(x,y,z) = \frac{1}{\theta}\delta(x-\ell_{x_\circ})\delta(y-\ell_{y_\circ})\delta(z-\ell_{z_\circ}), \tag{16}$$

where $\ell_{x_\circ}$, $\ell_{y_\circ}$, $\ell_{z_\circ}$ represent the x, y, z unbounded ($-\infty < \ell_{x_\circ}, \ell_{y_\circ}, \ell_{z_\circ} < \infty$) Cartesian coordinates of the virus point source, respectively; and δ is the Dirac delta function. It should be noted that here G represents the virus mass release from point source.

Instantaneous Virus Loading from a Point Source Geometry

For the case of instantaneous virus loading the mass release rate function is described by the following expression

$$G(t) = M\delta(t-t_\circ), \tag{17}$$

where M signifies the total virus mass released; and $t_\circ$ is the time of instantaneous virus release. Combining (12) and (15)–(17) yields

$$C(t,x,y,z) = \frac{M}{\theta}\left(\frac{1}{16\pi^2 D_x D_y}\right)^{1/2} \exp\left[\frac{U(x-\ell_{x_\circ})}{2D_x}\right]$$
$$\times \left[\mathcal{H}Q(t-t_\circ, x-\ell_{x_\circ}, y-\ell_{y_\circ}, z-\ell_{z_\circ}) + \frac{\partial Q(t-t_\circ, x-\ell_{x_\circ}, y-\ell_{y_\circ}, z-\ell_{z_\circ})}{\partial t}\right], \quad (18)$$

where the following property of Dirac delta function was employed

$$\int_{\alpha_1}^{\alpha_2} f_\circ(t)\delta(t-t_\circ)\, dt = f_\circ(t_\circ), \qquad \alpha_1 \le t_\circ \le \alpha_2, \quad (19)$$

and $f_\circ$ is an arbitrary function. The desired analytical solution for the case of instantaneous virus loading conditions is obtained by substituting (13) and (14) into (18), to yield

$$C(t,x,y,z) = \frac{M}{\theta}\int_0^{t-t_\circ}\left(\frac{1}{64\pi^3 D_x D_y D_z \zeta^3}\right)^{1/2}$$
$$\Lambda_1(t-t_\circ)\ \Lambda_2(t-t_\circ)\ \Lambda_3(\zeta, x-\ell_{x_\circ}, y-\ell_{y_\circ}, z-\ell_{z_\circ})\ d\zeta$$
$$+ \frac{M}{\theta}\left(\frac{1}{64\pi^3 D_x D_y D_z (t-t_\circ)^3}\right)^{1/2}$$
$$\Lambda_1(t-t_\circ)\ \Lambda_3(t-t_\circ, x-\ell_{x_\circ}, y-\ell_{y_\circ}, z-\ell_{z_\circ}), \quad (20)$$

where the following definitions were employed

$$\Lambda_1(t) = \exp\big[-\mathcal{H}t\big], \quad (21a)$$

$$\Lambda_2(t) = \left(\frac{\mathcal{B}\zeta}{t-\zeta}\right)^{1/2} I_1\Big[2\big(\mathcal{B}\zeta(t-\zeta)\big)^{1/2}\Big], \quad (21b)$$

$$\Lambda_3(t,x,y,z) = \exp\left[\frac{Ux}{2D_x} - \frac{1}{4t}\left(\frac{x^2}{D_x}+\frac{y^2}{D_y}+\frac{z^2}{D_z}\right) - t\left(\mathcal{A}+\frac{U^2}{4D_x}-\mathcal{H}\right)\right]. \quad (21c)$$

Continuous or Periodic Virus Loading from a Point Source Geometry

For the case of a continuous or temporally periodic virus loading, the mass release rate function can be represented by a generalized Fourier series (Hassani, 1991)

$$G(t) = \overline{\Omega} + \sum_{n=1}^{\infty} \Omega_n \exp\left[\frac{i2n\pi t}{t_p}\right], \tag{22}$$

where $\overline{\Omega}$ represents the mean value of the virus mass release rate from the source; Ω_n is a spectrum of known coefficients; n is the wave number; and t_p is the temporal period of fluctuation. It should be noted that for the special case of an infinite period ($t_p \to \infty$), (22) reduces to a constant rate source loading ($G = \overline{\Omega}$). In view of (19), combining (12) with (15), (16) and (22) yields

$$C(t,x,y,z) = \left(\frac{1}{16\pi^2 D_x D_y}\right)^{1/2} \int_0^t \exp\left[\frac{U(x-\ell_{x_o})}{2D_x}\right] \frac{G(t-\tau)}{\theta}$$

$$\times \left[\mathcal{H}Q(\tau, x-\ell_{x_o}, y-\ell_{y_o}, z-\ell_{z_o}) + \frac{\partial Q(\tau, x-\ell_{x_o}, y-\ell_{y_o}, z-\ell_{z_o})}{\partial \tau}\right] d\tau. \tag{23}$$

The desired analytical solution for continuous/periodic virus loading conditions is obtained by substituting (13) and (14) into (23), to yield

$$C(t,x,y,z) = \int_0^t \int_0^\tau \left(\frac{1}{64\pi^3 D_x D_y D_z \zeta^3}\right)^{1/2} \frac{G(t-\tau)}{\theta}$$

$$\Lambda_1(\tau)\ \Lambda_2(\tau)\ \Lambda_3(\zeta, x-\ell_{x_o}, y-\ell_{y_o}, z-\ell_{z_o})\ d\zeta\ d\tau$$

$$+ \int_0^t \left(\frac{1}{64\pi^3 D_x D_y D_z \tau^3}\right)^{1/2} \frac{G(t-\tau)}{\theta}$$

$$\Lambda_1(\tau)\ \Lambda_3(\tau, x-\ell_{x_o}, y-\ell_{y_o}, z-\ell_{z_o})\ d\tau. \tag{24}$$

Aquifer with Semi–infinite Thickness

The appropriate initial and boundary conditions for this aquifer, as illustrated schematically in Figure 1b, are (8)–(10) and the following semi–infinite vertical boundary conditions

$$\frac{\partial C(t,x,y,0)}{\partial z} = 0, \tag{25}$$

$$\frac{\partial C(t,x,y,\infty)}{\partial z} = 0, \tag{26}$$

where the boundary condition (25) represents a zero dispersive flux boundary and (26) preserves concentration continuity for a semi–infinite vertical aquifer thickness. The vertical level $z = 0$ defines the location of the water table or a confining layer. Equation (4) subject to conditions (8)–(10), (25), and (26) is solved analytically by straightforward but laborious procedures. It should be noted that z increases in the downward direction. Taking Laplace transforms with respect to time variable t and space variable z, and Fourier transforms with respect to space variables x and y of (4) and subsequently employing the transformed initial and boundary conditions, followed by inverse transformations yields the desired analytical solution for an aquifer with semi–infinite thickness (see Appendix B)

$$C(t,x,y,z) = \left(\frac{1}{64\pi^3 D_x D_y D_z}\right)^{1/2} \int_0^t \int_{-\infty}^{\infty} \int_{-\infty}^{\infty} \int_0^{\infty} F(t-\tau,q,v,p)\ \Lambda_1(\tau)$$

$$\times \left\{ \int_0^{\tau} \frac{\Lambda_2(\tau)}{\zeta^{3/2}}\ \Lambda_3(\zeta, x-q, y-v)\Big[\Lambda_4(\zeta, z+p) + \Lambda_4(\zeta, z-p)\Big]\ d\zeta \right.$$

$$\left. + \frac{\Lambda_3(\tau, x-q, y-v)}{\tau^{3/2}}\Big[\Lambda_4(\tau, z+p) + \Lambda_4(\tau, z-p)\Big] \right\} dp dv dq d\tau, \tag{27}$$

where the following definitions were employed

$$\Lambda_4(t,x,y) = \exp\left[\frac{Ux}{2D_x} - \frac{1}{4t}\left(\frac{x^2}{D_x} + \frac{y^2}{D_y}\right) - t\left(\mathcal{A} - \mathcal{H} + \frac{U^2}{4D_x}\right)\right], \tag{28a}$$

$$\Lambda_5(t,z) = \exp\left[\frac{-z^2}{4D_z t}\right]. \tag{28b}$$

Virus Source Configuration

In the semi–infinite thickness aquifer case, continuous/periodic virus loading from point as well as two–dimensional source geometries are considered.

Continuous/Periodic Virus Loading from a Point Source Geometry

Substituting (15) and (16) into (27) yields the analytical solution for the case of a point source geometry

$$C(t,x,y,z) = \left(\frac{1}{64\pi^3 D_x D_y D_z}\right)^{1/2} \int_0^t \frac{G(t-\tau)}{\theta}\ \Lambda_1(\tau) \times \left\{ \int_0^\tau \frac{\Lambda_2(\tau)}{\zeta^{3/2}}\ \Lambda_4(\zeta, x-\ell_{x_o}, y-\ell_{y_o}) \Big[\Lambda_5(\zeta, z+\ell_{z_o}) + \Lambda_5(\zeta, z-\ell_{z_o})\Big]\ d\zeta + \frac{\Lambda_4(\tau, x-\ell_{x_o}, y-\ell_{y_o})}{\tau^{3/2}} \Big[\Lambda_5(\tau, z+\ell_{z_o}) + \Lambda_5(\tau, z-\ell_{z_o})\Big] \right\} d\tau. \quad (29)$$

Continuous/Periodic Virus Loading from an Elliptic Source Geometry

The elliptic source geometry can be applied to represent virus sources such as land disposed sewage sludge, groundwater recharge by basin, and sanitary landfills, as described mathematically by the following expression

$$W(x,y,z) = \begin{cases} \dfrac{\delta(z-\ell_{z_o})}{\theta} & \dfrac{(x-\ell_{x_o})^2}{a^2} + \dfrac{(y-\ell_{y_o})^2}{b^2} \le 1, \\ 0 & \text{otherwise,} \end{cases} \quad (30)$$

where ℓ_{x_o}, ℓ_{y_o}, ℓ_{z_o} are x, y, z Cartesian coordinates, respectively, of the center of the elliptic source geometry, and a and b represent the semi–axes of the ellipse parallel to x– and y–axes, respectively.

Substituting (15) and (30) into (27) leads to the analytical solution for the case of an elliptic source geometry

$$C(t,x,y,z) = \left(\frac{1}{64\pi^2 D_x D_z}\right)^{1/2} \int_0^t \int_{a_1}^{a_2} \frac{G(t-\tau)}{\theta}\ \Lambda_1(\tau)$$

$$\times \left\{ \int_0^\tau \frac{\Lambda_2(\tau)}{\zeta}\ \Lambda_4(\zeta, x-q, 0)\Big[\Lambda_5(\zeta, z+\ell_{z_o}) + \Lambda_5(\zeta, z-\ell_{z_o})\Big]\ \Lambda_6(\zeta)\ d\zeta \right.$$

$$\left. + \frac{\Lambda_4(\tau, x-q, 0)}{\tau}\Big[\Lambda_5(\tau, z+\ell_{z_o}) + \Lambda_5(\tau, z-\ell_{z_o})\Big]\ \Lambda_6(\tau) \right\} dq d\tau, \quad (31)$$

where

$$\Lambda_6(t) = \operatorname{erf}\Big[\kappa_1(t,q,y)\Big] - \operatorname{erf}\Big[\kappa_2(t,q,y)\Big], \quad (32)$$

$$a_1 = \ell_{x_o} - a, \quad (33)$$

$$a_2 = \ell_{x_o} + a, \quad (34)$$

$$\kappa_1(t,q,y) = \left\{ y - \ell_{y_o} + \left[b^2 - \frac{b^2(q-\ell_{x_o})^2}{a^2} \right]^{1/2} \right\} \left(\frac{1}{4D_y t}\right)^{1/2}, \quad (35)$$

$$\kappa_2(t,q,y) = \left\{ y - \ell_{y_o} - \left[b^2 - \frac{b^2(q-\ell_{x_o})^2}{a^2} \right]^{1/2} \right\} \left(\frac{1}{4D_y t}\right)^{1/2}, \quad (36)$$

erf[ ] is the error function, and the following transformation and integral relationship were employed

$$\kappa = \frac{y-v}{(4tD_y)^{1/2}}, \qquad d\kappa = \frac{-dv}{(4tD_y)^{1/2}}, \quad (37a, b)$$

$$\int_{\kappa_1}^{\kappa_2} \exp[-\kappa^2]\ d\kappa = \frac{-\pi^{1/2}}{2}\Big\{\operatorname{erf}\big[\kappa_1\big] - \operatorname{erf}\big[\kappa_2\big]\Big\}. \quad (38)$$

As noted by Chrysikopoulos (1995), solving for an elliptic source geometry is advantageous because the appropriate solution for a circular source can easily be obtained by setting $a = b = r$ in (32)–(36), where r is the radius of the circular source.

Aquifer with Finite Thickness

The desired analytical solution for the case of an aquifer with finite thickness, as illustrated schematically in Figure 1c, is obtained by solving (4) subject to conditions (8)–(10), (25), and the following finite vertical, lower boundary condition,

$$\frac{\partial C(t,x,y,H)}{\partial z} = 0, \tag{39}$$

where H is the aquifer thickness. The boundary condition (39) implies that the aquifer is confined by an impermeable layer at depth $z = H$. Taking Laplace transform with respect to time variable t, Fourier transforms with respect to space variables x and y, and finite Fourier cosine transform with respect to space variable z of equation (4), and subsequently employing the transformed initial and boundary conditions, followed by inverse transformations yields (see Appendix C)

$$\begin{aligned} C(t,x,y,z) = & \left(\frac{1}{16\pi^2 D_x D_y}\right)^{1/2} \int_0^t \int_{-\infty}^{\infty} \int_{-\infty}^{\infty} \Lambda_1(\tau) \\ & \times \left\{ \int_0^\tau \frac{\Lambda_2(\tau)}{\zeta} \Lambda_4(\zeta, x-q, y-v)\ \Lambda_7\Big(\zeta, \ddot{F}(t-\tau,q,v,0), \ddot{F}(t-\tau,q,v,\psi_m)\Big)\, d\zeta \right. \\ & \left. + \frac{\Lambda_4(\tau, x-q, y-v)}{\tau} \Lambda_7\Big(\tau, \ddot{F}(t-\tau,q,v,0), \ddot{F}(t-\tau,q,v,\psi_m)\Big) \right\} dv dq d\tau, \end{aligned} \tag{40}$$

where

$$\Lambda_7(t, f_1, f_2) = \frac{f_1}{H} + \frac{2}{H} \sum_{m=1}^{\infty} f_2 \exp\left[-\psi_m^2 D_z t\right] \cos\left(\psi_m z\right), \tag{41}$$

$$\psi_m = \frac{m\pi}{H}, \tag{42}$$

m is the integer summation index, $\ddot{F}(t,x,y,\psi_m)$ represents the finite Fourier cosine transform of $F(t,x,y,z)$ with respect to space variable z with corresponding finite Fourier cosine transform variable ψ_m, and f_1 and f_2 are arbitrary functions.

Virus Source Configuration

In the finite thickness aquifer case, continuous/periodic virus loading from point as well as two–dimensional source geometries are considered.

Continuous/Periodic Virus Loading from a Point Source Geometry

The desired analytical solution for the case of point source geometry is obtained by substituting the corresponding expression for $\ddot{F}(t,x,y,\psi_m)$ into (40). Substituting (16) into (15) and subsequently taking the finite Fourier cosine transform with respect to space variable z of the resulting expression yields

$$\begin{aligned}\ddot{F}(t,x,y,\psi_m) &= \int_0^H \frac{G(t)}{\theta}\delta(x-\ell_{x_o})\delta(y-\ell_{y_o})\delta(z-\ell_{z_o})\cos(\psi_m z)\,dz \\ &= \frac{G(t)}{\theta}\delta(x-\ell_{x_o})\delta(y-\ell_{y_o})\cos(\psi_m \ell_{z_o}),\end{aligned} \tag{43}$$

where the latter formulation in (43) is a consequence of employing (19). In view of (43) and (19) the general solution (40) reduces to the following form

$$\begin{aligned}C(t,x,y,z) = \left(\frac{1}{16\pi^2 D_x D_y}\right)^{1/2} &\int_0^t \frac{G(t-\tau)}{\theta}\,\Lambda_1(\tau) \\ &\times \left\{\int_0^\tau \frac{\Lambda_2(\tau)}{\zeta}\,\Lambda_4(\zeta, x-\ell_{x_o}, y-\ell_{y_o})\,\Lambda_7\Big(\zeta,1,\cos(\psi_m\ell_{z_o})\Big)\,d\zeta\right. \\ &\left. + \frac{\Lambda_4(\tau, x-\ell_{x_o}, y-\ell_{y_o})}{\tau}\,\Lambda_7\Big(\tau,1,\cos(\psi_m\ell_{z_o})\Big)\right\} d\tau.\end{aligned} \tag{44}$$

Continuous/Periodic Virus Loading from an Elliptic Source Geometry

In view of (30) the finite Fourier cosine transform of (15) with respect to z is given by

$$\ddot{F}(t,x,y,\psi_m) = \begin{cases} \dfrac{G(t)}{\theta}\cos(\psi_m\ell_{z_o}) & \dfrac{(x-\ell_{x_o})^2}{a^2} + \dfrac{(y-\ell_{y_o})^2}{b^2} \le 1, \\ 0 & \text{otherwise.}\end{cases} \tag{45}$$

Substituting (45) into (40), the desired analytical solution for the case of elliptic source geometry is as follows

$$C(t,x,y,z) = \left(\frac{1}{16\pi D_x}\right)^{1/2} \int_0^t \int_{a_1}^{a_2} \frac{G(t-\tau)}{\theta}\, \Lambda_1(\tau) \times \left\{ \int_0^\tau \frac{\Lambda_2(\tau)}{\zeta^{1/2}}\, \Lambda_4(\zeta, x-q, 0)\, \Lambda_6(\zeta)\, \Lambda_7\Big(\zeta, 1, \cos\left(\psi_m \ell_{z_o}\right)\Big)\, d\zeta + \frac{\Lambda_4(\tau, x-q, 0)}{\tau^{1/2}}\, \Lambda_6(\tau)\, \Lambda_7\Big(\tau, 1, \cos\left(\psi_m \ell_{z_o}\right)\Big) \right\} dq\, d\tau. \tag{46}$$

Virus Attachment onto the Solid Matrix

Nonequilibrium Virus Adsorption (S MODEL)

Assuming that the adsorption process consists of virus diffusion to the outer layer of a solid particle by nonequilibrium mass transfer and virus immobilization onto the solid particle while in equilibrium with the liquid phase virus concentration in the outer layer, the expression for accumulation of adsorbed viruses (2) can be replaced by (Sim and Chrysikopoulos, 1996)

$$\frac{\rho}{\theta}\frac{\partial C^*(t,x,y,z)}{\partial t} = k\Big[C(t,x,y,z) - C_g(t,x,y,z)\Big] - \lambda^* \frac{\rho}{\theta} C^*(t,x,y,z), \tag{47}$$

where k is the mass transfer rate constant; and C_g is the liquid phase concentration of virus in direct contact with solids. Furthermore, it is assumed that the following linear equilibrium relationship is valid

$$C^*(t,x,y,z) = K_d C_g(t,x,y,z), \tag{48}$$

where K_d is the partition or distribution coefficient. In view of (2), (47), and (48) the following substitutions

$$r_1 = k, \tag{49}$$

$$r_2 = \frac{k}{K_d}, \tag{50}$$

can be employed into (20), (24), (29), (31), (44), or (46) to yield the corresponding S model solutions for each combination of virus source loading and geometry for different aquifer types.

Virus Filtration (C MODEL)

Assuming that the colloid filtration theory is applicable to virus attachment onto the solid matrix of a subsurface formation, the accumulation of filtered viruses can be written as

$$\frac{\rho}{\theta}\frac{\partial C^*(t,x,y,z)}{\partial t} = k_c C(t,x,y,z) - k_r \frac{\rho}{\theta} C^*(t,x,y,z) - \lambda^* \frac{\rho}{\theta} C^*(t,x,y,z), \tag{51}$$

where C^* is now the virus concentration retained in the porous medium by the filtration process; k_c is the clogging rate constant; and k_r is the declogging rate constant. In view of (2) and (51) the following substitutions

$$r_1 = k_c, \tag{52}$$

$$r_2 = \frac{k_r \rho}{\theta}, \tag{53}$$

can be employed into (20), (24), (29), (31), (44), or (46) to yield the corresponding C model solutions for each combination of virus source loading and geometry for different aquifer types.

Model simulations under nonequilibrium virus adsorption (S model) as well as virus filtration (C model) conditions are performed for a variety of virus source configurations. The integrals present in the analytical solutions are evaluated numerically by the integration routines Q1DA and QDAG, which utilize globally adaptive quadrature algorithms (IMSL, 1991; Kahaner, 1989). The infinite series part of the solution for the case of an aquifer with finite thickness (41) is evaluated by considering up to 1000 terms (m=1000). The groundwater table and the bottom of the finite thickness aquifer are assumed to be located at $z = 0$ cm and $z = H = 6$ cm, respectively. For simplicity, the values for M and $\overline{\Omega}$ are set to unity. Unless otherwise specified, the fixed parameter values used in the simulations are those listed in Table 1. Furthermore, the concentrations generated under continuous virus loading conditions are normalized by the steady state concentration evaluated at $t = 100$ d (C_∞) as suggested by Hunt (1978).

Table 1. Model Parameters for Simulations

Parameter	Value	Reference
D_x	15 cm^2/hr	Sim and Chrysikopoulos (1995)
$D_y = D_z$	1.13 cm^2/hr	Goltz and Roberts (1986)
K_d	20 ml/g	Vilker (1981)
$\lambda = \lambda^*$	0 d	
ρ	1.5 g/cm^3	Yates and Ouyang (1992)
θ	0.25	Park et al. (1992)

Two–dimensional snapshots of virus concentration simulated by the C model under instantaneous point source conditions for an aquifer with infinite thickness (eqs. 20, 52, 53) at three successive times are illustrated in Figure 2. The viruses are assumed to be highly conservative ($k_c = k_r = \lambda = \lambda^* \simeq 0$). As the center of mass moves downstream from the source, enhanced but symmetric spreading is observed in both longitudinal and lateral directions.

The general behavior of the S model is similar to the C model. For example, Figure 3 illustrates two–dimensional snapshots of virus concentrations on the x, y plane, at three successive times as predicted by the S model under continuous but constant ($G = \overline{\Omega}$) point source conditions for an aquifer with infinite thickness (eqs. 24, 49, 50). For the case examined here, the virus loading is continuous as opposed to instantaneous loading considered in Figures 2. It should be noted that the elongation of the virus plume in Figure 3 along the longitudinal direction is caused by the assumption $D_x > D_y$.

Figure 4 illustrates two–dimensional snapshots of virus concentration at three successive times simulated by S model for an aquifer with semi–infinite thickness (eqs. 29, 49, 50). A point source is assumed to be located inside the aquifer at $\ell_{x_o} = 20$ cm, $\ell_{y_o} = 0$ cm, $\ell_{z_o} = 3$ cm. It is observed that as the virus plume spreads with increasing time, viruses accumulate at the groundwater table ($z = 0$ cm), whereas no accumulation of viruses occurs anywhere else below the water table because the aquifer extends to infinity without boundary (eq. 26). Consequently, the observed virus plume is asymmetric with respect to the flow direction along the plume centerline. In contrast, Figure 5 illustrates symmetric virus plumes at three successive times, as predicted by S model for an aquifer with finite thickness and point source geometry (eqs. 44, 49, 50). This is due to the presence of a fixed impermeable lower boundary (eq. 39) in addition to the upper groundwater table boundary. Virus accumulation progressively increases not

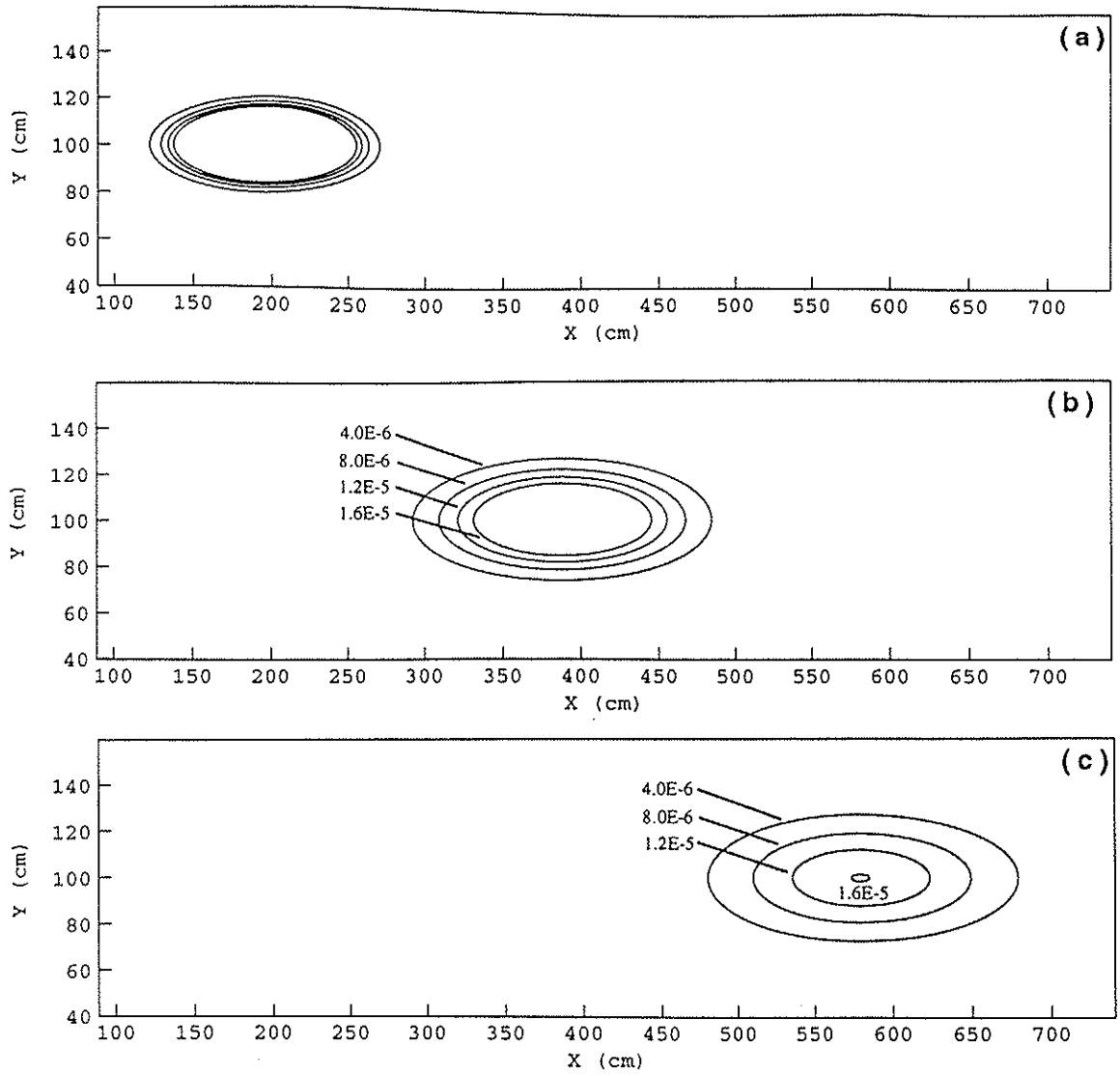

Figure 2: Concentration contours in the x, y plane obtained by the C model under instantaneous loading of highly conservative viruses at (a) $t = 1.0$ d, (b) $t = 3.0$ d, and (c) $t = 5.0$ d (Here $z = 100$ cm, $k_c = k_r = 0$ hr^{-1}, and $U = 4$ cm/hr).

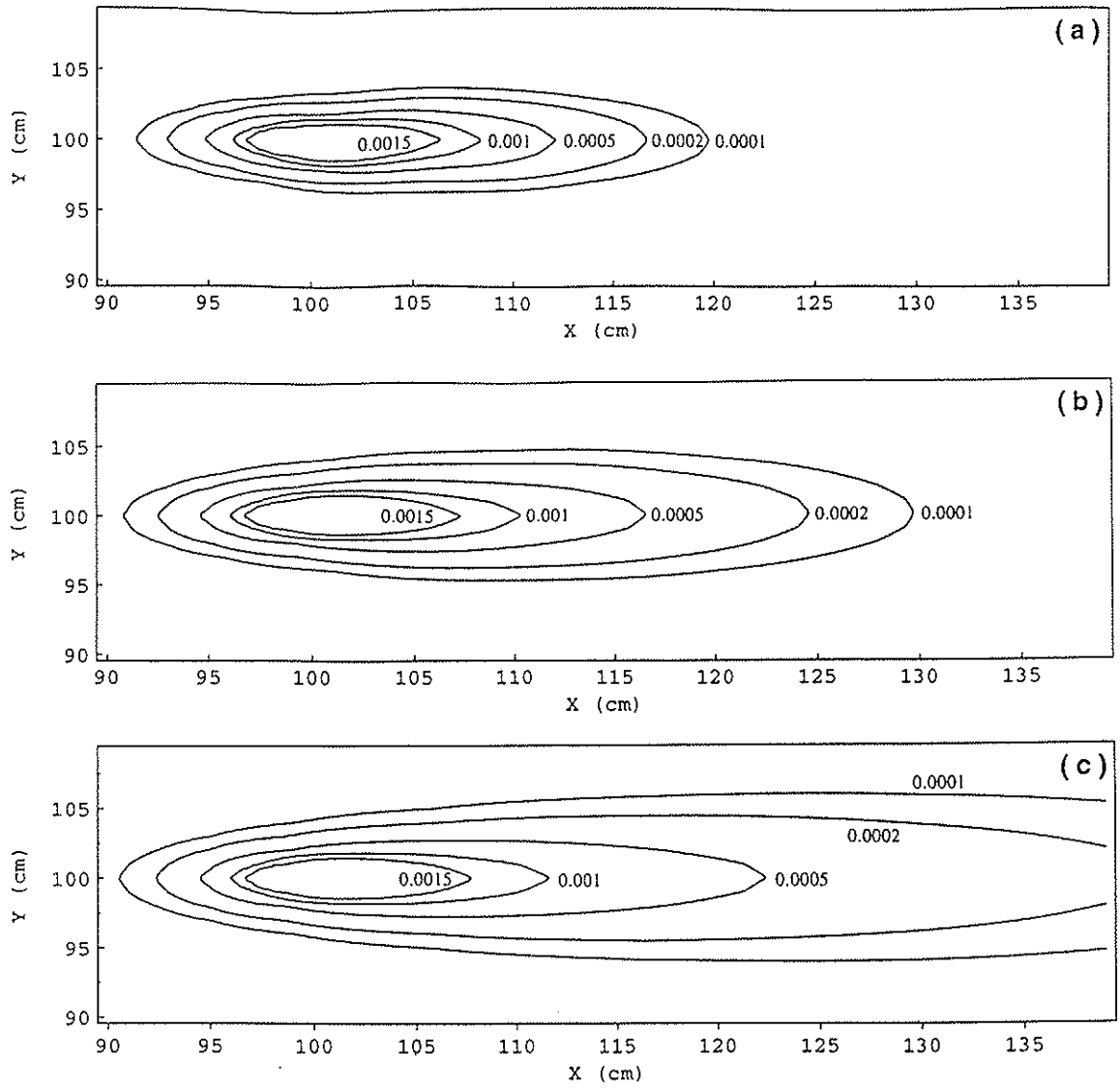

Figure 3: Concentration contours in the x, y plane obtained by the S model under continuous virus loading conditions at (a) $t = 0.1$ d, (b) $t = 0.2$ d, and (c) $t = 0.5$ d, (Here $z = 100$ cm, $k = 0.0001$ hr^{-1}, and $U = 4$ cm/hr).

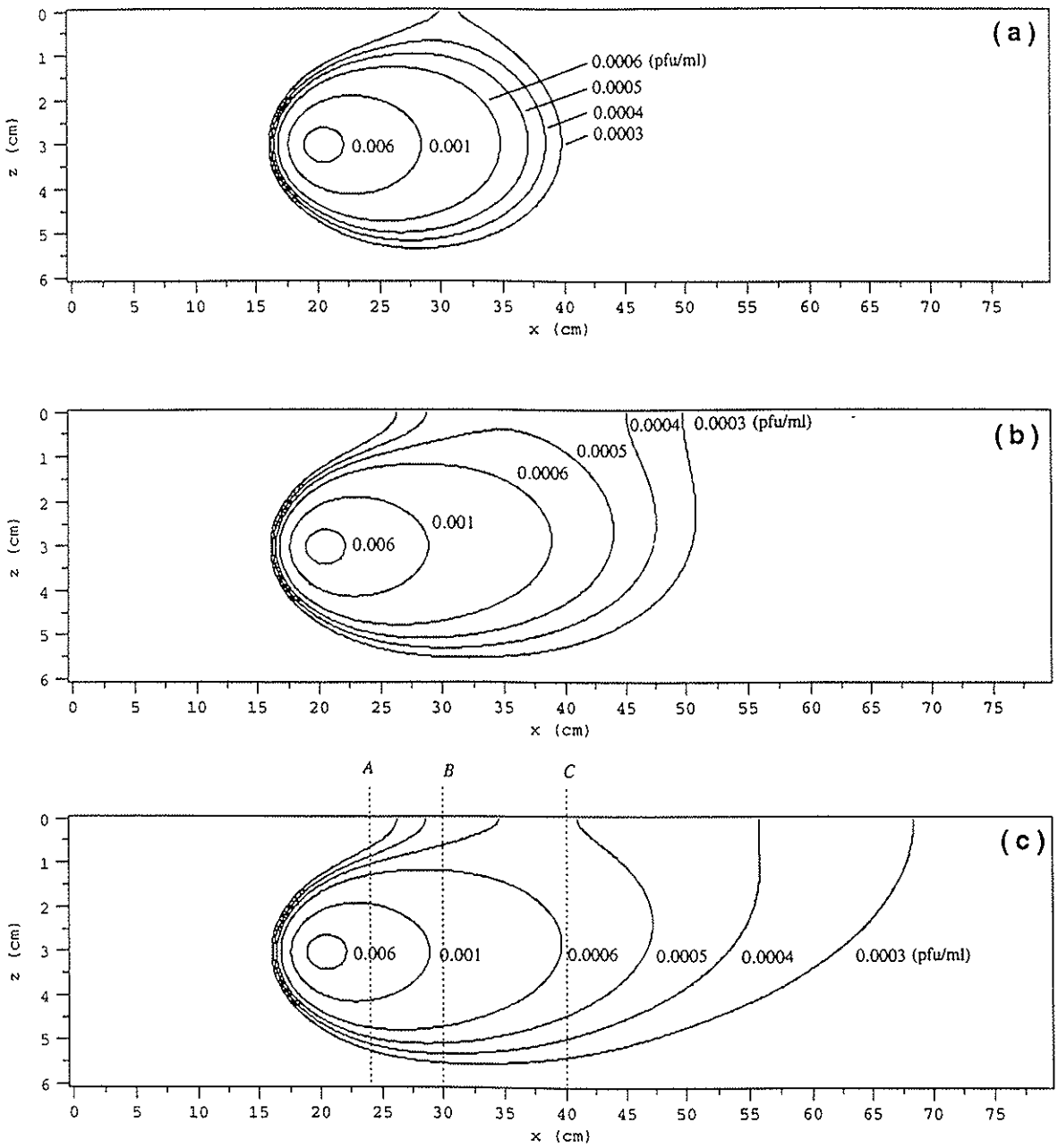

Figure 4: Concentration contours in the x, z plane obtained by the S model with point source under semi–infinite vertical boundary condition at (a) $t = 0.1$ d, (b) $t = 0.2$ d, and (c) $t = 0.5$ d (Here $\ell_{x_o} = 20$ cm, $\ell_{y_o} = 0$ cm, $\ell_{z_o} = 3$ cm, $y = 0$ cm, $k = 0.0006$ hr^{-1}, and $U = 8$ cm/hr).

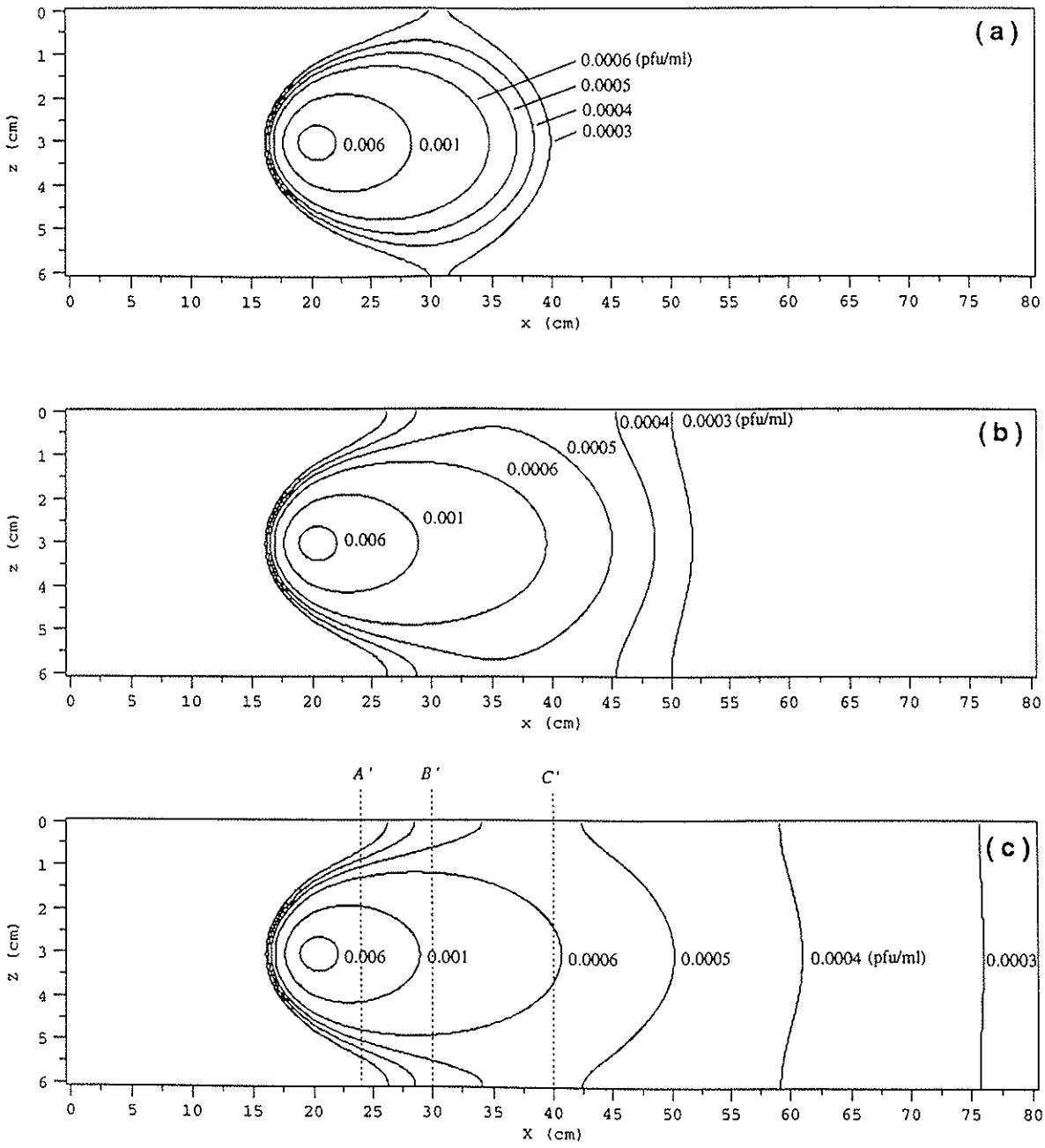

Figure 5: Concentration contours in the x, z plane obtained by the S model with point source under finite vertical boundary condition at (a) $t = 0.1$ d, (b) $t = 0.2$ d, and (c) $t = 0.5$ d (Here $\ell_{x_o} = 20$ cm, $\ell_{y_o} = 0$ cm, $\ell_{z_o} = 3$ cm, $y = 0$ cm, $k = 0.0006$ hr^{-1}, and $U = 8$ cm/hr).

only at the groundwater table ($z = 0$ cm) but also at the fixed impermeable boundary ($z = H = 6$ cm). Comparing Figures 4 and 5, it is clear that the vertical migration of viruses is hindered by the two fixed boundaries. Furthermore, the presence of these boundaries contributes to the enhancement of virus transport downstream from the source in the direction of groundwater flow.

In order to clearly demonstrate the different effects of the semi–infinite and finite vertical aquifer domains on virus transport, concentration profiles are predicted along the vertical cross sections A, B and C (shown in Figure 4c), and A', B' and C' (shown in Figure 5c) and they are presented together in Figure 6. At $x = 24$ cm (cross sections A and A', see Figure 6a), the difference in concentration levels simulated for the two different sets of boundary conditions examined here is insignificant since the plume spreading in vertical direction is relatively small and thus the majority of viruses are still concentrated near the plume centerline. However, with increasing distance from the source (see Figures 6b and 6c), due to increased spreading of the virus plume, the model for the aquifer with finite vertical thickness predicts a considerable accumulation of viruses both at the upper ($z = 0$ cm) and lower ($z = 6$ cm) boundaries, whereas for the case of a semi–infinite aquifer, viruses continue to spread vertically downward. Therefore, the difference between the two model simulations becomes more pronounced. These results suggest that the presence of a shallow impermeable boundary may significantly influence virus concentrations.

The effect of the lower impermeable boundary condition is also demonstrated for the case of an elliptic source geometry. Two-dimensional snapshots of virus concentrations at $t = 0.1$ d are predicted by S model with an elliptic source geometry for an aquifer with semi–infinite thickness (eqs. 31, 49, 50, Figure 7a) as well as for an aquifer with finite thickness (eqs. 46, 49, 50, Figure 7b). Similarly to the case of point source geometry, the presence of a shallow impermeable aquitard significantly constricts the

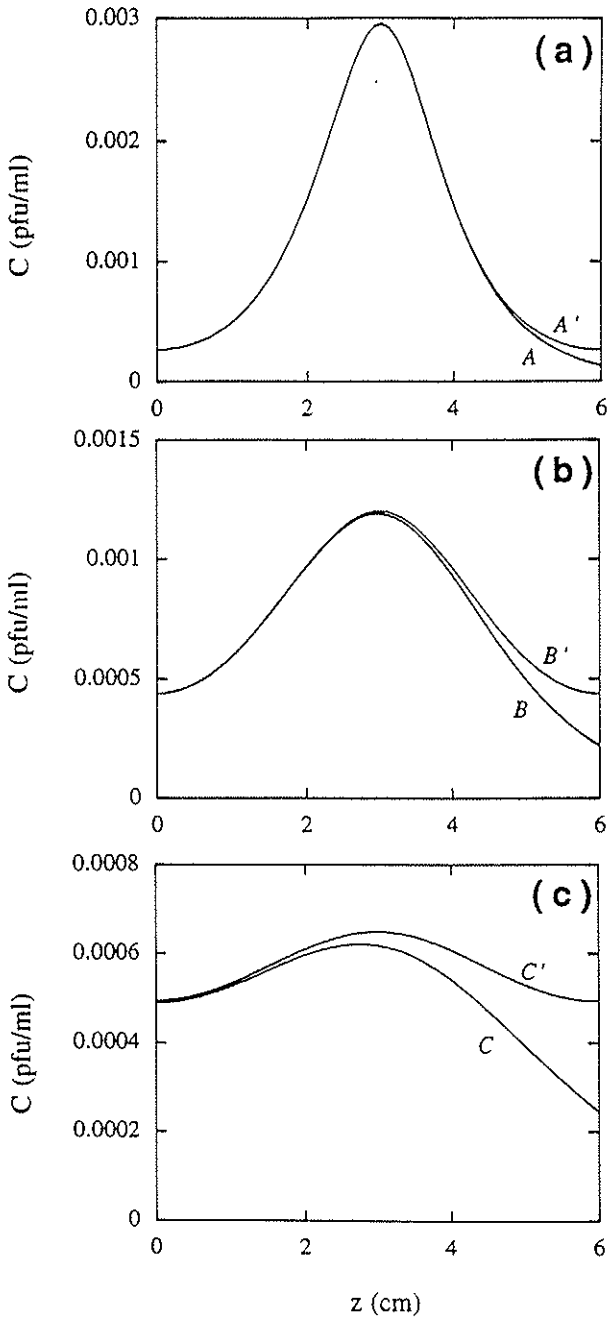

Figure 6: Concentration snapshots obtained by S model with point source under semi–infinite and finite vertical boundary conditions along the cross sections (a) A and A' ($x = 24$ cm), (b) B and B' ($x = 30$ cm), and (c) C and C' ($x = 40$ cm) shown in Figures 4c and 5c (Here $y = 0$ cm, $k = 0.0006$ hr^{-1}, and $U = 8$ cm/hr).

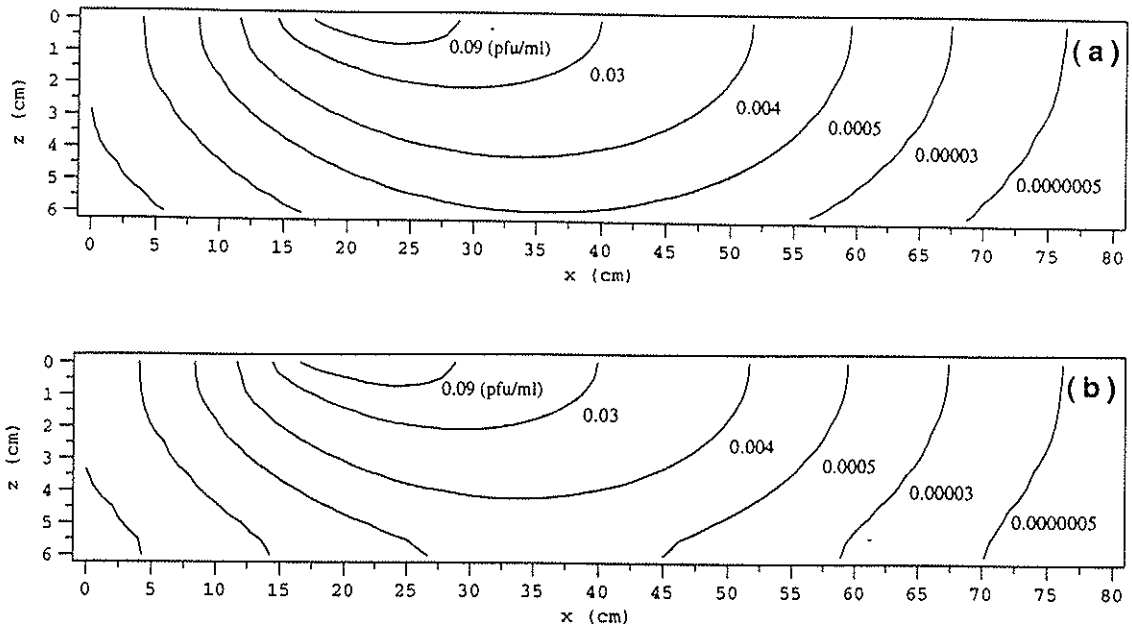

Figure 7: Concentration contours in the x, z plane obtained by the S model with elliptic source at $t = 0.1$ d under (a) semi–infinite and (b) finite vertical boundary conditions (Here $\ell_{x_o} = 20$ cm, $\ell_{y_o} = 0$ cm, $\ell_{z_o} = 0$ cm, $y = 0$ cm, $a = b = 5$ cm, $k = 0.0006$ hr^{-1}, and $U = 8$ cm/hr).

vertical spreading of viruses, which consequently leads to an enhanced virus migration in the direction of groundwater flow.

Governing Equations

The transient virus transport through one–dimensional, homogeneous, saturated porous media, accounting for virus adsorption and inactivation, is governed by the following partial differential equation (Sim and Chrysikopoulos, 1995)

$$\frac{\partial C(t,x)}{\partial t}+\frac{\rho}{\theta}\frac{\partial C^*(t,x)}{\partial t}=D\frac{\partial^2 C(t,x)}{\partial x^2}-U\frac{\partial C(t,x)}{\partial x}-\lambda(t)C(t,x)-\lambda^*(t)\frac{\rho}{\theta}C^*(t,x), \quad (54)$$

where the accumulation of adsorbed viruses is represented by (47)–(50).

Time Dependent Inactivation

In the present work, inactivation rate coefficients are considered to be time dependent, and consequently the inactivation of viruses in the liquid phase and solid phase are described by the following modified first–order rate expressions

$$\frac{dC(t)}{dt}=-\lambda(t)C(t), \quad (55)$$

$$\frac{dC^*(t)}{dt}=-\lambda^*(t)C^*(t), \quad (56)$$

respectively, where the time dependent inactivation rate coefficients of viruses in the respective phases are described by

$$\lambda(t)=\lambda_\circ e^{-\alpha t}, \quad (57)$$

$$\lambda^*(t)=\lambda^*_\circ e^{-\alpha^* t}, \quad (58)$$

where $\lambda_\circ$ and $\lambda^*_\circ$ are the initial inactivation rate coefficients of viruses in the respective phases; and α and α^* are the resistivity coefficients of viruses in the respective phases.

The magnitude of α is proportional to the resistivity of the dominant subpopulation, because the overall inactivation is controlled by the dominant subpopulation. The inactivation rate coefficients of viruses in the liquid phase are assumed to be twice as large as the coefficients of adsorbed viruses ($\lambda_\circ^* = \lambda_\circ/2$) (Reddy et al., 1981; Yates and Ouyang, 1992). Furthermore, the resistivity coefficient of adsorbed viruses is considered to be equal to the resistivity coefficient of viruses in the liquid phase ($\alpha^* = \alpha$). Substituting (57) into (55) and solving the resulting expression subject to the initial condition $C(0) = C_i$, where C_i is the initial liquid phase virus concentration, yields

$$\ln\left[\frac{C(t)}{C_i}\right] = \frac{\lambda_\circ}{\alpha}\left(e^{-\alpha t} - 1\right). \tag{59}$$

The parameters $\lambda_\circ$ and α can be obtained by fitting the preceding equation to existing experimental data.

Table 2. Estimated Virus Inactivation Parameters for Three Data Sets

Parameter	Poliovirus (1°C) (Hurst et al., 1980)	Bacteriophage-λ ($\simeq$ 15° C) (Grant et al., 1993)	Bacteriophage-λ^{++} (60° C) (Parkinson and Huskey, 1971)
		Time Dependent Inactivation	
$\lambda_\circ$ (d^{-1})	0.25	2.66	226.02
α (d^{-1})	0.42	2.41	24.65
sse	0.68	0.27	1.67
		Constant Inactivation	
λ (d^{-1})	0.018	0.17	32.28
sse	2.45	0.40	26.71

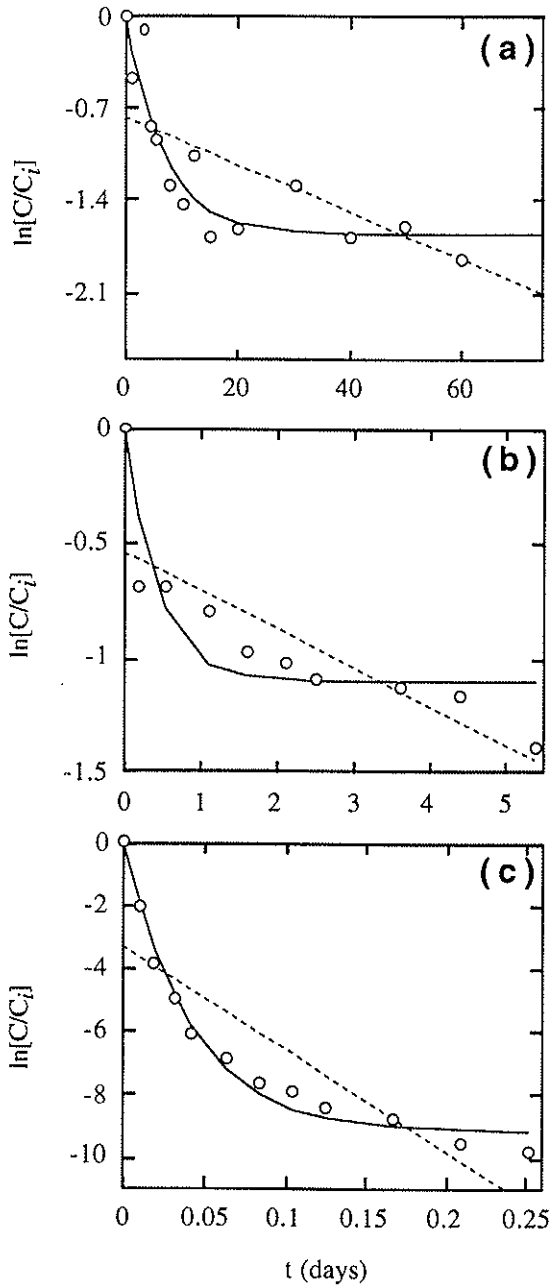

Figure 8: Batch inactivation experimental data (circles) for (a) *Poliovirus* at 1 °C with distilled water under anaerobic conditions adopted from Hurst et al. (1980), (b) *bacteriophage*–λ at $\simeq$ 15 °C with 10 mM NaCl electrolyte and pH 7 under aerobic conditions adopted from Grant et al. (1993), and (c) *bacteriophage*–λ^{++} at 60 °C with 10mM $MgSO_4$ under aerobic conditions adopted from Parkinson and Huskey (1971), and simulated concentration history based on the pseudo first–order inactivation model (solid curves) and constant rate inactivation model (dashed lines).

Figure 8 presents virus inactivation experimental data fitted by both (8) and the constant inactivation rate model ($\lambda(t) = \lambda$). The estimated parameters for both inactivation rate models considered together with the corresponding residual sums of squared error (sse) are listed in Table 2. Clearly, the pseudo first–order inactivation rate model simulates the experimental data much better than the constant inactivation rate model, which fails to match the data at early and late times (see Figure 8). The slope of a tangent to a solid curve represents the inactivation rate coefficient at the particular time.

Initial/Boundary Conditions

The appropriate initial and boundary conditions for a semi–infinite, one–dimensional porous formation in the presence of a continuous source of viruses are (Sim and Chrysikopoulos, 1995):

$$C(0,x) = C^*(0,x) = 0, \tag{60}$$

$$-D\frac{\partial C(t,0)}{\partial x} + UC(t,0) = UC_\circ, \tag{61}$$

$$\frac{\partial C(t,\infty)}{\partial x} = 0, \tag{62}$$

where $C_\circ$ is the source concentration. The condition (60) establishes that there is no initial liquid phase and adsorbed virus concentrations within the porous medium. The constant flux boundary condition (61) implies virus concentration discontinuity at the inlet. The downstream boundary condition (62) preserves concentration continuity for a semi–infinite system. The governing virus transport equation (54) in conjunction with the relationships (53), (54), (57), and (58) is solved numerically subject to initial/boundary conditions (60)–(62). The numerical solution is obtained by using the IMSL one–dimensional partial differential equation (PDE) solver MOLCH (IMSL, 1991).

Model Simulations

The effect of temporally variable inactivation on liquid phase virus concentration in saturated porous media is investigated by conducting model simulations. The fixed parameter values used for virus transport simulations are: $D = 32.04$ cm^2/hr and $U = 5.04$ cm/hr (Bales et al., 1991); $K_d = 2.08 \times 10^{-2}$ ml/mg (Vilker, 1981); $k = 1.2$ hr^{-1} (Vilker and Burge, 1980); $\rho = 1.5$ g/cm^3 (Yates and Ouyang, 1992); and $\theta = 0.25$ (Park et al., 1992). The pseudo first–order inactivation rate parameters are estimated from the experimental data collected by Grant et al. (1993) (see Figure 8b).

At early time, the simulated concentration profile for the case of pseudo first–order inactivation is lower than the one for the case of constant inactivation rate (see Figure 9a), whereas at late time the concentration levels are reversed (see Figure 9b). The temporally variable inactivation allows rapid inactivation of the most sensitive subpopulations at early time, and extended survival of the most resistive subpopulations at late time. Therefore, viruses may remain infective in porous media for an extended period of time and thus travel farther downstream from the source.

Parameter Sensitivity Analysis

In order to investigate the response of the virus transport model to perturbations of the pseudo first–order inactivation parameters α and λ_o, a formal parameter sensitivity analysis is conducted. A parameter sensitivity coefficient that represents the degree of spatial and temporal change in the dependent variable (i.e., concentration) due to the fluctuation of a particular model parameter, was obtained by differentiating the dependent variable with respect to the parameter of interest (Koda et al., 1979; Knopman and Voss, 1987).

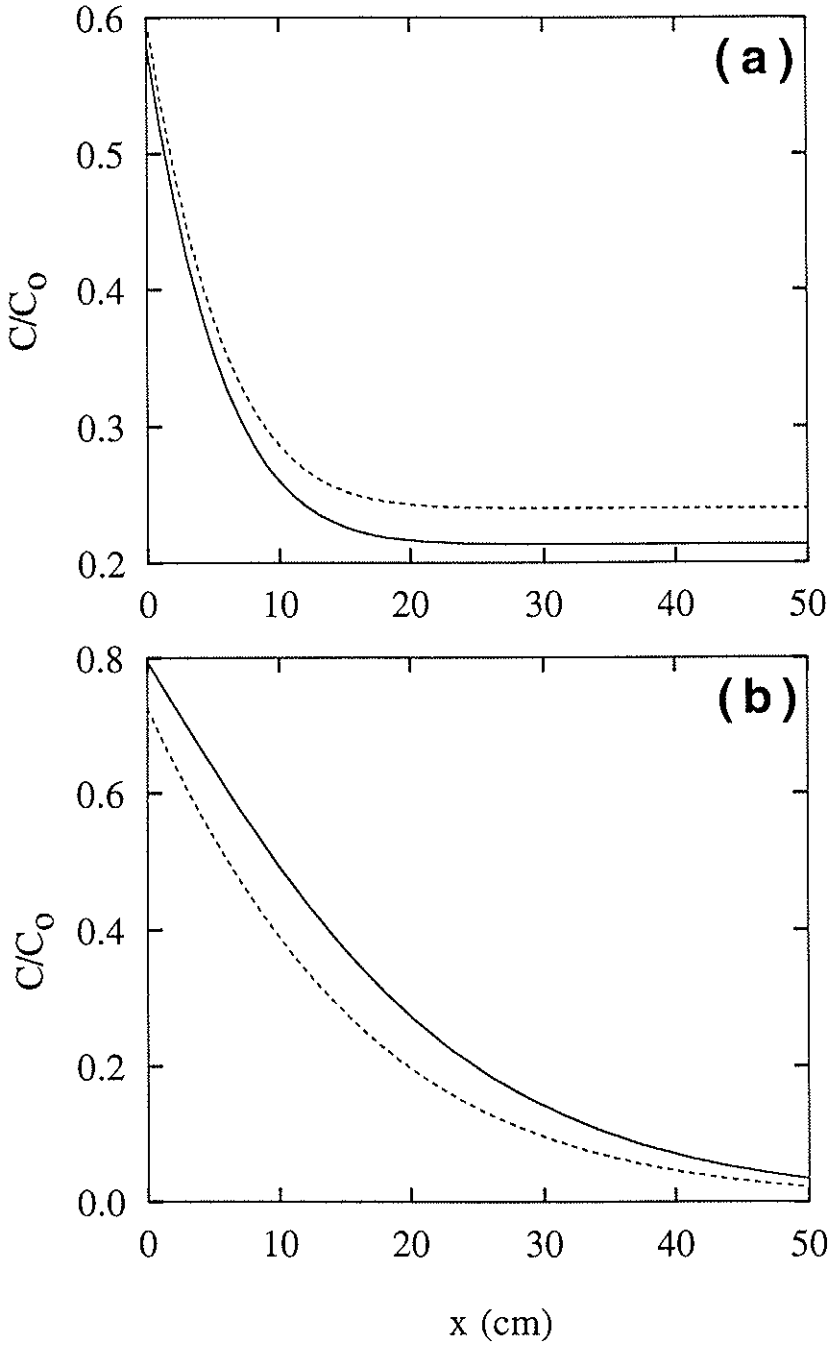

Figure 9: Liquid phase virus concentration snapshots for pseudo first–order (solid curves) or constant rate (dashed curves) inactivation at (a) t=0.05 d and (b) t=10 d.

The sensitivity coefficients with respect to the resistivity coefficient for liquid phase and adsorbed virus concentrations are given by

$$Z_\alpha(t,x) = \frac{\partial C(t,x)}{\partial \alpha}, \qquad Z^*_\alpha(t,x) = \frac{\partial C^*(t,x)}{\partial \alpha}, \tag{63a, b}$$

respectively. Differentiating the governing equations (1)–(3) with respect to α yields

$$\frac{\partial Z_\alpha(t,x)}{\partial t} + \frac{\rho}{\theta}\frac{\partial Z^*_\alpha(t,x)}{\partial t} = D\frac{\partial^2 Z_\alpha}{\partial x^2} - U\frac{\partial Z_\alpha}{\partial x} + \lambda(t)\Big[tC(t,x) - Z_\alpha(t,x)\Big] - \lambda^*(t)\frac{\rho}{\theta}Z^*_\alpha(t,x), \tag{64}$$

$$\frac{\rho}{\theta}\frac{\partial Z^*_\alpha(t,x)}{\partial t} = k\left[Z_\alpha(t,x) - \frac{Z^*_\alpha(t,x)}{K_d}\right] - \lambda^*(t)\frac{\rho}{\theta}Z^*_\alpha(t,x). \tag{65}$$

Similarly, the corresponding initial and boundary conditions are obtained from (60)–(62) as follows

$$Z_\alpha(0,x) = Z^*_\alpha(0,x) = 0, \tag{66}$$

$$-D\frac{\partial Z_\alpha(t,0)}{\partial x} + UZ_\alpha(t,0) = 0, \tag{67}$$

$$\frac{\partial Z_\alpha(t,\infty)}{\partial x} = 0. \tag{68}$$

The sensitivity coefficients Z_α and Z^*_α are evaluated by solving (64) and (65) subject to (66)–(68) together with the governing equations (54) and (47)–(50) subject to conditions (60)–(62). A numerical solution is obtained by the IMSL one–dimensional PDE solver MOLCH (IMSL, 1991).

The sensitivity coefficients with respect to the initial inactivation rate coefficient for liquid phase and adsorbed virus concentrations are given by

$$Z_{\lambda_\circ}(t,x) = \frac{\partial C(t,x)}{\partial \lambda_\circ}, \qquad Z^*_{\lambda_\circ}(t,x) = \frac{\partial C^*(t,x)}{\partial \lambda_\circ}, \tag{69a, b}$$

respectively. The desired partial differential equations are obtained in a fashion similar to the case of resistivity coefficient

$$\frac{\partial Z_{\lambda_\circ}(t,x)}{\partial t} + \frac{\rho}{\theta}\frac{\partial Z^*_{\lambda_\circ}(t,x)}{\partial t} = D\frac{\partial^2 Z_{\lambda_\circ}}{\partial x^2} - U\frac{\partial Z_{\lambda_\circ}}{\partial x} - e^{-\alpha t}C(t,x) - \lambda(t)Z_{\lambda_\circ}(t,x) - \lambda^*(t)\frac{\rho}{\theta}Z^*_{\lambda_\circ}(t,x), \tag{70}$$

$$\frac{\rho}{\theta}\frac{\partial Z^*_{\lambda_\circ}(t,x)}{\partial t} = k\left[Z_{\lambda_\circ}(t,x) - \frac{Z^*_{\lambda_\circ}(t,x)}{K_d}\right] - \lambda^*(t)\frac{\rho}{\theta}Z^*_{\lambda_\circ}(t,x). \tag{71}$$

The sensitivity coefficients $Z_{\lambda_\circ}$ and $Z^*_{\lambda_\circ}$ are evaluated by solving numerically (70) and (71) subject to conditions (66)–(68) with substitution of Z_α and Z^*_α by $Z_{\lambda_\circ}$ and $Z^*_{\lambda_\circ}$, in conjunction with the governing equations (54) and (47)–(50) subject to conditions (60)–(62).

Figure 10a shows that at different locations within the one–dimensional porous medium, Z_α approaches a zero value with increasing time, because the system reaches a steady state, where $C(t,x)$ is insensitive to variations in α. The impact of α on liquid phase virus concentration is most significant near the source. However, it should be noted that although the peak value of Z_α decreases with increasing distance from the source, the time interval over which α influences the liquid phase concentration increases with increasing distance from the source. The spatial variation of Z_α at different simulation times is illustrated in Figure 10b. It is observed that the peak value of Z_α progressively decreases with increasing time, because the system approaches a steady state. Therefore, liquid phase virus concentrations are highly sensitive to α near the source and during early stages of virus transport. The temporal and spatial variations of the sensitivity coefficient $Z_{\lambda_\circ}$ exhibit similar trends to the ones observed for Z_α in Figure 10.

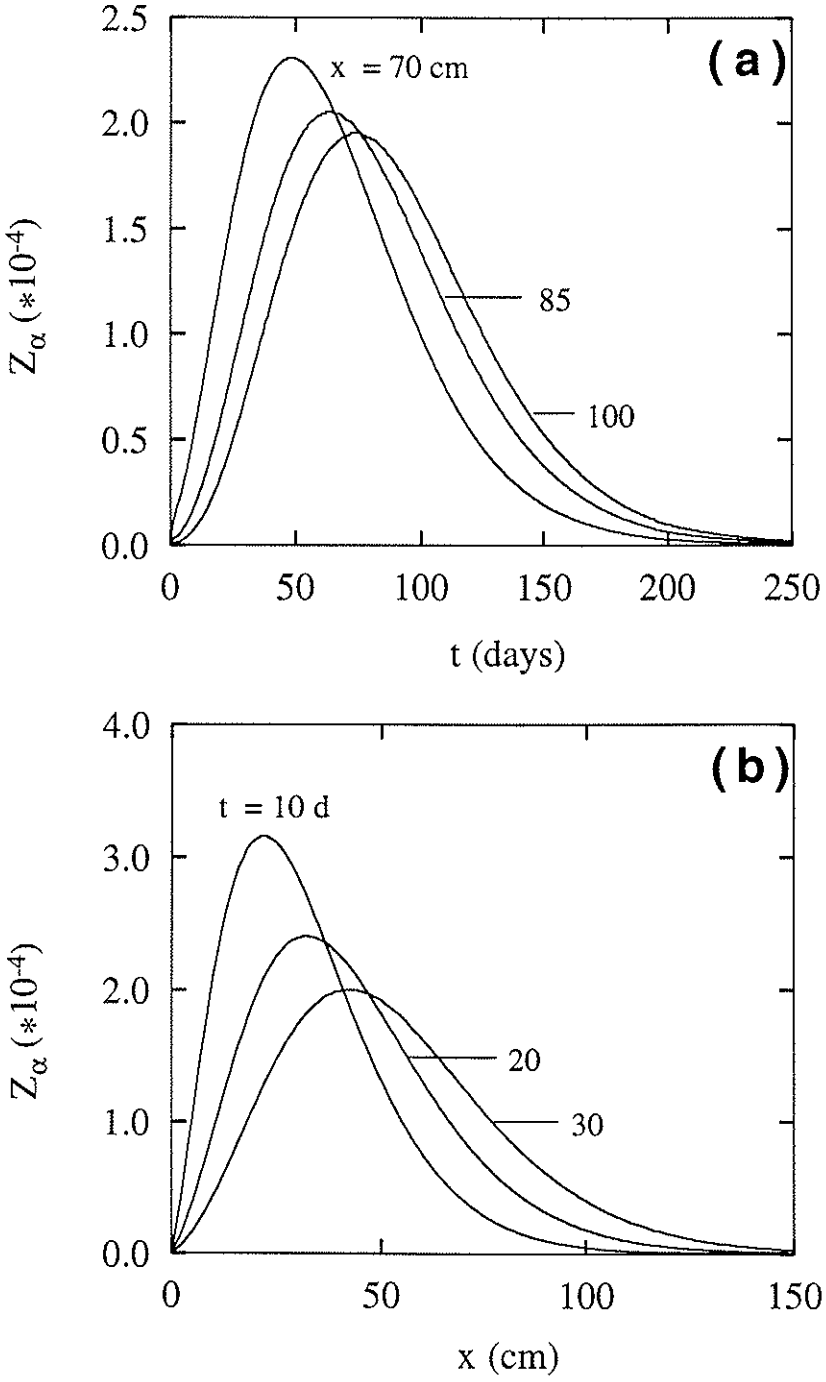

Figure 10: Variation of Z_α as a function of (a) time and (b) space.

Analytical models for virus transport in saturated, homogeneous porous media were developed, accounting for three–dimensional hydrodynamic dispersion in a uniform flow field, first–order inactivation of liquid phase and deposited viruses with different inactivation rate coefficients, and virus attachment onto the solid matrix of the porous formation by either nonequilibrium adsorption (S model) or modified colloid filtration (C model). The governing transport equations were solved analytically by employing Laplace, Fourier, and finite Fourier cosine transform techniques. Aquifers with either infinite, semi–infinite or finite thickness are considered. The derived analytical solutions are general enough to accommodate a variety of source loadings and virus source geometries. The simulations presented in this study are based on an instantaneous or continuous source loading from either point source or elliptic source geometry. It was shown that virus transport in subsurface porous media is significantly influenced by the aquifer boundary conditions. For an aquifer confined by a shallow impermeable aquitard, virus migration in the vertical direction is restricted whereas virus transport in the direction of groundwater flow is enhanced, compared to the case of a relatively thick aquifer. The present work focused on developing virus transport models useful for a variety of practical applications. Therefore, the analytical models developed here are particularly useful for preliminary estimation of virus migration, characterization of virus contamination sources, examination of possible aquifer boundary conditions, validation of numerical solutions, and determination of virus transport parameters from laboratory or well defined field experiments.

A model for one–dimensional virus transport in saturated, homogeneous porous media is developed, accounting for inactivation of liquid phase and adsorbed viruses with different time dependent inactivation rate coefficients which are represented by

functional relationships determined from experimental data. The significant impact of temporally variable inactivation rate coefficients on virus transport was demonstrated by model simulations. It was concluded from a formal parameter sensitivity analysis that virus transport data collected in the vicinity of the source of contamination at early time are most reliable for estimation of inactivation rate coefficients. The model is particularly useful for improving our understanding of virus inactivation processes in conjunction with studying virus transport through packed columns under controlled laboratory conditions. The applicability of this model to field investigations is limited to relatively homogeneous subsurface formations. The methodology of this work can provide a starting point for generalization to multidimensional virus transport in heterogeneous porous or fractured media.

Derivation of the Analytical Solution for an Aquifer with Infinite Thickness

The desired analytical solution is obtained by solving the problem described by the following integrodifferential equation and initial/boundary conditions

$$\frac{\partial C(t,x,y,z)}{\partial t} - D_x\frac{\partial^2 C(t,x,y,z)}{\partial x^2} - D_y\frac{\partial^2 C(t,x,y,z)}{\partial y^2} - D_z\frac{\partial^2 C(t,x,y,z)}{\partial z^2}$$

$$+ U\frac{\partial C(t,x,y,z)}{\partial x} + \mathcal{A}C(t,x,y,z) - \mathcal{B}\int_0^t C(\tau,x,y,z)e^{-\mathcal{H}(t-\tau)}d\tau = F(t,x,y,z), \quad \text{(A1)}$$

$$C(0,x,y,z) = 0, \quad \text{(A2)}$$

$$C(t,\pm\infty,y,z) = 0, \quad \text{(A3)}$$

$$C(t,x,\pm\infty,z) = 0, \quad \text{(A4)}$$

$$C(t,x,y,\pm\infty) = 0. \quad \text{(A5)}$$

Taking Laplace transform with respect to time variable t and Fourier transforms with respect to space variables x, y, and z of equation (A1) and subsequently employing transformed initial condition (A2) yields

$$\hat{\tilde{\tilde{C}}}(s,\gamma,\omega,\phi) = \frac{\hat{\tilde{\tilde{F}}}(s,\gamma,\omega,\phi)}{\gamma^2 D_x + i\gamma U + E}, \quad \text{(A6)}$$

where

$$E = \omega^2 D_y + \phi^2 D_z + \mathcal{A} + s - \frac{\mathcal{B}}{s+\mathcal{H}}, \quad \text{(A7)}$$

and the following properties were employed for the Laplace and Fourier transformations (Roberts and Kaufman, 1966; Kreyszig, 1993)

$$\tilde{C}(s,x,y,z) = \int_0^\infty C(t,x,y,z)e^{-st}dt, \quad \text{(A8)}$$

$$\hat{\tilde{C}}(s,\gamma,y,z) = \frac{1}{(2\pi)^{1/2}}\int_{-\infty}^{\infty}\tilde{C}(s,x,y,z)e^{-i\gamma x}dx, \quad \text{(A9)}$$

$$\bar{\bar{\hat{C}}}(s,\gamma,\omega,z) = \frac{1}{(2\pi)^{1/2}} \int_{-\infty}^{\infty} \hat{\bar{C}}(s,\gamma,y,z) e^{-i\omega y} dy, \tag{A10}$$

$$\dot{\bar{\hat{C}}}(s,\gamma,\omega,\phi) = \frac{1}{(2\pi)^{1/2}} \int_{-\infty}^{\infty} \bar{\bar{\hat{C}}}(s,\gamma,\omega,z) e^{-i\phi z} dz, \tag{A11}$$

where the tilde signifies Laplace transform and s is the Laplace domain variable; the hat, overbar, and overdot signify Fourier transforms with respect to space variables x, y, and z with corresponding Fourier domain variables γ, ω, and ϕ, respectively; and $i = (-1)^{1/2}$.

The Fourier inverse transformation of (A6) with respect to γ is

$$\begin{aligned}
\dot{\bar{\tilde{C}}}(s,x,\omega,\phi) &= \frac{1}{(2\pi)^{1/2}} \mathcal{F}^{-1}\left\{\dot{\bar{\hat{F}}}(s,\gamma,\omega,\phi)\right\} * \mathcal{F}^{-1}\left\{\frac{1}{\gamma^2 D_x + i\gamma U + E}\right\} \\
&= \frac{\dot{\bar{\hat{F}}}(s,x,\omega,\phi)}{(2\pi)^{1/2}} * \left(\frac{1}{(2\pi)^{1/2}} \int_{-\infty}^{\infty} \frac{e^{i\gamma x}}{\gamma^2 D_x + i\gamma U + E}\, d\gamma\right) \\
&= \frac{\dot{\bar{\hat{F}}}(s,x,\omega,\phi)}{2\pi D_x} * \left(\int_{-\infty}^{\infty} \frac{\cos\gamma x}{\gamma^2 + \frac{i\gamma U}{D_x} + \frac{E}{D_x}}\, d\gamma + \int_{-\infty}^{\infty} \frac{i\sin\gamma x}{\gamma^2 + \frac{i\gamma U}{D_x} + \frac{E}{D_x}}\, d\gamma\right),
\end{aligned} \tag{A12}$$

where $\mathcal{F}^{-1}$ is the Fourier inverse operator; the asterisk represents convolution with respect to space variable x; and the following definitions of the Fourier inverse transform were employed

$$\mathcal{F}^{-1}\left\{\hat{f}_1(\gamma)\right\} = \frac{1}{(2\pi)^{1/2}} \int_{-\infty}^{\infty} \hat{f}_1(\gamma) e^{i\gamma x} d\gamma, \tag{A13}$$

$$\mathcal{F}^{-1}\left\{\hat{f}_1(\gamma)\hat{f}_2(\gamma)\right\} = \frac{f_1(x) * f_2(x)}{(2\pi)^{1/2}} = \frac{1}{(2\pi)^{1/2}} \int_{-\infty}^{\infty} f_1(x-\xi) f_2(\xi)\, d\xi, \tag{A14}$$

where f_1 and f_2 are arbitrary functions of x; and ξ is a dummy integration variable. It should be noted, however, that the latter expression in (A12) is a consequence of employing Euler's formula

$$e^{i\gamma x} = \cos\gamma x + i\sin\gamma x. \tag{A15}$$

In view of (A14) and the following integral identities (Gradshteyn and Ryzhik, 1980, eq. 3.724.1 & 2, p. 407)

$$\int_{-\infty}^{\infty} \frac{\sin\gamma x}{\gamma^2 + \beta\gamma + \alpha^2}\, d\gamma = -\pi\left(\alpha^2 - \frac{\beta^2}{4}\right)^{-1/2} \sin\left(\frac{\beta x}{2}\right) \exp\left[-x\left(\alpha^2 - \frac{\beta^2}{4}\right)^{1/2}\right], \tag{A16}$$

$$\int_{-\infty}^{\infty} \frac{\cos\gamma x}{\gamma^2+\beta\gamma+\alpha^2}\, d\gamma = \pi\left(\alpha^2-\frac{\beta^2}{4}\right)^{-1/2}\cos\left(\frac{\beta x}{2}\right)\exp\left[-x\left(\alpha^2-\frac{\beta^2}{4}\right)^{1/2}\right], \quad \text{(A17)}$$

the expression (A12) is simplified as

$$\begin{aligned}\dot{\tilde{\tilde{C}}}(s,x,\omega,\phi) &= \frac{\dot{\tilde{\tilde{F}}}(s,x,\omega,\phi)}{2\pi D_x} * \left\{\Psi\left[\cos\left(\frac{iUx}{2D_x}\right) - i\sin\left(\frac{iUx}{2D_x}\right)\right]\right\} \\ &= \frac{\dot{\tilde{\tilde{F}}}(s,x,\omega,\phi)}{2\pi D_x} * \left\{\Psi\exp\left[\frac{Ux}{2D_x}\right]\right\}, \end{aligned} \quad \text{(A18)}$$

where

$$\Psi = \pi\left(\frac{E}{D_x}+\frac{U^2}{4D_x^2}\right)^{-1/2}\exp\left[-x\left(\frac{E}{D_x}+\frac{U^2}{4D_x^2}\right)^{1/2}\right], \quad \text{(A19)}$$

and the latter expression in (A18) is obtained by using the following complex trigonometric functions (Kreyszig, 1993, p.737)

$$\cos\left(\frac{iUx}{2D_x}\right) = \frac{1}{2}\left\{\exp\left[\frac{Ux}{2D_x}\right] + \exp\left[-\frac{Ux}{2D_x}\right]\right\}, \quad \text{(A20a)}$$

$$\sin\left(\frac{iUx}{2D_x}\right) = \frac{i}{2}\left\{\exp\left[\frac{Ux}{2D_x}\right] - \exp\left[-\frac{Ux}{2D_x}\right]\right\}. \quad \text{(A20b)}$$

In view of (A13), (A14), and (A19), the expression (A18) is written as

$$\dot{\tilde{\tilde{C}}}(s,x,\omega,\phi) = \int_{-\infty}^{\infty} \dot{\tilde{\tilde{F}}}(s,q,\omega,\phi)\; f(s,x-q,\omega,\phi)\; dq, \quad \text{(A21)}$$

where

$$f(s,x,\omega,\phi) = \left(\frac{1}{4D_xD_y\left(\omega^2+\mathcal{S}\right)}\right)^{1/2}\exp\left[\frac{Ux}{2D_x}\right]\exp\left[-x\left(\left(\omega^2+\mathcal{S}\right)\frac{D_y}{D_x}\right)^{1/2}\right], \quad \text{(A22)}$$

$$\mathcal{S} = \frac{1}{D_y}\left(\phi^2 D_z + \mathcal{A} + s - \frac{\mathcal{B}}{s+\mathcal{H}} + \frac{U^2}{4D_x}\right). \quad \text{(A23)}$$

In view of (A13), (A14), and (A22), the Fourier inverse transformation of (A21) with respect to ω is given by

$$\dot{\tilde{C}}(s,x,y,\phi) = \left(\frac{1}{16\pi^2 D_xD_y}\right)^{1/2}\int_{-\infty}^{\infty}\exp\left[\frac{U(x-q)}{2D_x}\right]\left\{\dot{\tilde{F}}(s,q,y,\phi) * \int_{-\infty}^{\infty}\Phi e^{i\omega y}d\omega\right\}dq$$

$$= \left(\frac{1}{16\pi^2 D_x D_y}\right)^{1/2} \int_{-\infty}^{\infty} \exp\left[\frac{U(x-q)}{2D_x}\right]$$

$$\times \left\{ \dot{\tilde{F}}(s,q,y,\phi) * \left[\int_{-\infty}^{\infty} \Phi \cos(\omega y) d\omega + \int_{-\infty}^{\infty} i\Phi \sin(\omega y) d\omega \right] \right\} dq, \qquad \text{(A24)}$$

where

$$\Phi = \left(\frac{1}{\omega^2 + \mathcal{S}}\right)^{1/2} \exp\left[-(x-q)\left(\left(\omega^2 + \mathcal{S}\right)\frac{D_y}{D_x}\right)^{1/2}\right], \qquad \text{(A25)}$$

and the latter expression in (A24) is a consequence of employing (15). It should be noted that Φ as well as $\cos(\omega y)$ are even functions of ω, whereas $\sin(\omega y)$ is an odd function of ω. Therefore, the trigonometric integrals are evaluated as follows

$$\int_{-\infty}^{\infty} \Phi \cos(\omega y)\ d\omega = 2\int_{0}^{\infty} \Phi \cos(\omega y)\ d\omega = 2K_\circ\left[\mathcal{S}^{1/2}\left(y^2 + \frac{(x-q)^2 D_y}{D_x}\right)^{1/2}\right], \qquad \text{(A26)}$$

$$\int_{-\infty}^{\infty} i\Phi \sin(\omega y)\ d\omega = 0, \qquad \text{(A27)}$$

where $K_\circ$ is the modified Bessel function of the second kind of zeroth order; and the following integral identity was utilized in (A26) (Gradshteyn and Ryzhik, 1980, eq. 3.961.2, p. 498)

$$\int_{0}^{\infty} \frac{\cos(\omega y)}{\left(\omega^2 + \alpha^2\right)^{1/2}} \exp\left[-\beta\left(\omega^2 + \alpha^2\right)^{1/2}\right]\ d\omega = K_\circ\left[\alpha\left(y^2 + \beta^2\right)^{1/2}\right]. \qquad \text{(A28)}$$

In view of (A26), (A27) and application of the convolution theorem, (A24) reduces to

$$\dot{\tilde{C}}(s,x,y,\phi) = \int_{-\infty}^{\infty}\int_{-\infty}^{\infty} \dot{\tilde{F}}(s,q,v,\phi)\ g(s,x-q,y-v,\phi)\ dv\ dq, \qquad \text{(A29)}$$

where

$$g(s,x,y,\phi) = \left(\frac{1}{4\pi^2 D_x D_y}\right)^{1/2} \exp\left[\frac{Ux}{2D_x}\right] K_\circ\left[\mathcal{S}^{1/2}\left(y^2 + \frac{x^2 D_y}{D_x}\right)^{1/2}\right]. \qquad \text{(A30)}$$

In view of (A13), (A14), (A23) and (A30), the Fourier inverse transformation of (A29) with respect to ϕ is given by

$$\widetilde{C}(s,x,y,z) = \left(\frac{1}{16\pi^4 D_x D_y}\right)^{1/2} \int_{-\infty}^{\infty}\int_{-\infty}^{\infty} \exp\left[\frac{U(x-q)}{2D_x}\right]$$
$$\times \left\{ \widetilde{F}(s,q,v,z) * \int_{-\infty}^{\infty} K_\circ\Big[\mathcal{N}(s,x-q,y-v,\phi)\Big] e^{i\phi z} d\phi \right\} \, dv \, dq$$
$$= \left(\frac{1}{16\pi^4 D_x D_y}\right)^{1/2} \int_{-\infty}^{\infty}\int_{-\infty}^{\infty} \exp\left[\frac{U(x-q)}{2D_x}\right]$$
$$\times \left\{ \widetilde{F}(s,q,v,z) * \left[\int_{-\infty}^{\infty} K_\circ\Big[\mathcal{N}(s,x-q,y-v,\phi)\Big] \cos(\phi z)\, d\phi \right.\right.$$
$$\left.\left. + \int_{-\infty}^{\infty} K_\circ\Big[\mathcal{N}(s,x-q,y-v,\phi)\Big] i\sin(\phi z)\, d\phi \right] \right\} dv\, dq, \quad \text{(A31)}$$

where the following substitutions were employed

$$\mathcal{N}(s,x,y,\phi) = \Big[\phi^2 + \mathcal{N}_1(s)\Big]^{1/2} \mathcal{N}_2(x,y), \quad \text{(A32)}$$

$$\mathcal{N}_1(s) = \frac{1}{D_z}\left(\mathcal{A} + s - \frac{\mathcal{B}}{s+\mathcal{H}} + \frac{U^2}{4D_x}\right), \quad \text{(A33)}$$

$$\mathcal{N}_2(x,y) = \left(\frac{y^2 D_z}{D_y} + \frac{x^2 D_z}{D_x}\right)^{1/2}, \quad \text{(A34)}$$

and the latter expression in (A31) is a consequence of employing (A15). It should be noted that $\mathcal{N}$ and $\cos(\phi z)$ are even functions of ϕ, whereas $\sin(\phi z)$ is an odd function of ϕ. Therefore,

$$\int_{-\infty}^{\infty} K_\circ\Big[\mathcal{N}(s,x,y,\phi)\Big] \cos(\phi z)\, d\phi = 2\int_{0}^{\infty} K_\circ\Big[\mathcal{N}(s,x,y,\phi)\Big] \cos(\phi z)\, d\phi$$
$$= \left(\frac{\pi^2}{\mathcal{N}_2^2 + z^2}\right)^{1/2} \exp\left[-\mathcal{N}_1^{1/2}\Big(\mathcal{N}_2^2 + z^2\Big)^{1/2}\right], \quad \text{(A35)}$$

$$\int_{-\infty}^{\infty} iK_\circ\Big[\mathcal{N}(s,x,y,\phi)\Big] \sin(\phi z)\, d\phi = 0, \quad \text{(A36)}$$

where the following integral identity was employed in (A35) (Gradshteyn and Ryzhik, 1980, eq. 6.677.5, p. 736)

$$\int_0^\infty K_\circ\left[\alpha\left(\phi^2+\beta^2\right)^{1/2}\right]\cos(\phi z)\,d\phi = \frac{1}{2}\left(\frac{\pi^2}{\alpha^2+z^2}\right)^{1/2}\exp\left[-\beta\left(\alpha^2+z^2\right)^{1/2}\right]. \quad \text{(A37)}$$

In view of (A35), (A36), and application of the convolution theorem, (A31) reduces to

$$\widetilde{C}(s,x,y,z) = \int_{-\infty}^{\infty}\int_{-\infty}^{\infty}\int_{-\infty}^{\infty}\widetilde{F}(s,q,v,p)\;h(s,x-q,y-v,z-p)\;dp\;dv\;dq, \quad \text{(A38)}$$

where

$$h(s,x,y,z) = h_1(s,x,y,z)\;h_2(x,y,z), \quad \text{(A39)}$$

$$h_1(s,x,y,z) = \exp\left[-\mathcal{N}_1^{1/2}\left(\mathcal{N}_2^2+z^2\right)^{1/2}\right], \quad \text{(A40)}$$

$$h_2(x,y,z) = \left[\frac{1}{16\pi^2 D_x D_y\left(\mathcal{N}_2^2+z^2\right)}\right]^{1/2}\exp\left[\frac{Ux}{2D_x}\right]. \quad \text{(A41)}$$

Furthermore, for mathematical convenience, let

$$h_1 = \frac{\mathcal{H}h_1}{s+\mathcal{H}} + \frac{sh_1}{s+\mathcal{H}}. \quad \text{(A42)}$$

The inverse Laplace transform of (A38) with respect to s can be found by employing the following relationship

$$\mathcal{L}^{-1}\left\{\frac{1}{s+\mathcal{H}}\widetilde{f}_\circ\left(s+\mathcal{H}-\frac{d}{s+\mathcal{H}}\right)\right\} = e^{-\mathcal{H}t}\int_0^t I_\circ\left[2\left(d\zeta(t-\zeta)\right)^{1/2}\right]f_\circ(\zeta)\,d\zeta, \quad \text{(A43)}$$

where $\mathcal{L}^{-1}$ is the Laplace inverse operator; $\widetilde{f}_\circ(s)$ is the Laplace transform of the arbitrary function $f_\circ(t)$; and d is an arbitrary constant. Equation (A43) was obtained from the inverse Laplace transform pair reported by Lapidus and Amundson (1952) modified by direct application of the Bessel function relationship $I_\circ[\eta] = J_\circ[i\eta]$, where $J_\circ$ is the Bessel function of the first kind of zeroth order, and η is an arbitrary argument (Abramowitz and Stegun, 1972, eq. 9.6.3, p. 375). In view of (A33), (A34), and (A40), $\widetilde{f}_\circ(s)$ is assumed to be of the following form

$$\widetilde{f}_\circ(s) = \exp\left[-d_1(s+d_2)^{1/2}\right], \quad \text{(A44)}$$

where d_1 and d_2 are arbitrary constants. Furthermore, the inverse Laplace transform of $\widetilde{f}_\circ(s)$ is (Roberts and Kaufman, 1966)

$$f_\circ(t) = \mathcal{L}^{-1}\Big\{ \exp\Big[-d_1(s+d_2)^{1/2}\Big] \Big\} = \frac{d_1}{(4\pi t^3)^{1/2}} \exp\Big[\frac{-d_1^2}{4t} - d_2 t\Big]. \tag{A45}$$

Equation (A44) can also be used to express h_1 as

$$h_1 = \widetilde{f}_\circ\left(s+\mathcal{H}-\frac{d}{s+\mathcal{H}}\right) = \exp\left[-\frac{d_1}{(s+\mathcal{H})^{1/2}}\left\{s^2 + s(2\mathcal{H}+d_2) + \mathcal{H}(\mathcal{H}+d_2) - d\right\}^{1/2}\right]. \tag{A46}$$

Substitution of (A33) into (A40) yields

$$h_1 = \exp\left[-\left(\frac{\mathcal{N}_2^2+z^2}{D_z(s+\mathcal{H})}\right)^{1/2}\left\{s^2 + s\left(\mathcal{H}+\mathcal{A}+\frac{U^2}{4D_x}\right) + \mathcal{H}\left(\mathcal{A}+\frac{U^2}{4D_x}\right) - \mathcal{B}\right\}^{1/2}\right]. \tag{A47}$$

The unknown constants d, d_1, and d_2 are obtained by simple comparison of (A46) and (A47)

$$d = \mathcal{B}, \tag{A48}$$

$$d_1 = \left(\frac{\mathcal{N}_2^2+z^2}{D_z}\right)^{1/2}, \tag{A49}$$

$$d_2 = \mathcal{A} + \frac{U^2}{4D_x} - \mathcal{H}. \tag{A50}$$

In view of (A43), (A45), and (A48)–(A50), the following inverse Laplace transform is derived

$$\mathcal{L}^{-1}\left\{\frac{h_1}{s+\mathcal{H}}\right\} = \mathcal{P}(t,x,y,z), \tag{A51}$$

where

$$\begin{aligned}\mathcal{P}(t,x,y,z) =& e^{-\mathcal{H}t}\int_0^t I_\circ\Big[2\big(\mathcal{B}\zeta(t-\zeta)\big)^{1/2}\Big]\left(\frac{\mathcal{N}_2^2+z^2}{4\pi D_z\zeta^3}\right)^{1/2} \\ & \times \exp\left[-\frac{\mathcal{N}_2^2+z^2}{4D_z\zeta} - \zeta\left(\mathcal{A}+\frac{U^2}{4D_x}-\mathcal{H}\right)\right] d\zeta.\end{aligned} \tag{A52}$$

Furthermore, the following Laplace transform property (Kreysizig, 1993, eq. 6.2, p. 317)

$$\mathcal{L}\left\{\frac{\partial\mathcal{P}(t,x,y,z)}{\partial t}\right\} = s\widetilde{\mathcal{P}}(s,x,y,z) - \mathcal{P}(0,x,y,z), \tag{A53}$$

where $\mathcal{L}$ is the Laplace transform operator, together with $\mathcal{P}(0,x,y,z)=0$ suggests that

$$\mathcal{L}^{-1}\left\{\frac{sh_1}{s+\mathcal{H}}\right\}=\mathcal{L}^{-1}\left\{s\widetilde{\mathcal{P}}(s,x,y,z)\right\}=\frac{\partial\mathcal{P}(t,x,y,z)}{\partial t}. \tag{A54}$$

In view of (A42), (A51) and (A54), the inverse Laplace transformation of (A38) is given by

$$C(t,x,y,z)=\int_0^t\int_{-\infty}^{\infty}\int_{-\infty}^{\infty}\int_{-\infty}^{\infty}F(t-\tau,q,v,p)\;h_2(x-q,y-v,z-p)$$
$$\times\left[\mathcal{H}\mathcal{P}(\tau,x-q,y-v,z-p)+\frac{d\mathcal{P}(\tau,x-q,y-v,z-p)}{d\tau}\right]\;dp\;dv\;dq\;d\tau, \tag{A55}$$

where the following inverse Laplace transform relationship was employed

$$\mathcal{L}^{-1}\left\{\widetilde{f}_1(s)\widetilde{f}_2(s)\right\}=f_1(t)*f_2(t)=\int_0^t f_1(t-\tau)f_2(\tau)\;d\tau. \tag{A56}$$

Backsubstituting (A34), (A41) and (A52) into (A55) yields the desired generalized analytical solution (12)–(14).

APPENDIX B:

Derivation of the Analytical Solution for an Aquifer with Semi–Infinite Thickness

The analytical solution for the case of semi–infinite thickness is obtained by solving (4) subject to (8)–(10), (25), and (26). Taking Laplace transforms with respect to time variable t and space variable z and Fourier transforms with respect to space variables x and y of equation (4) and subsequently employing (8) and transformed boundary condition (25) yields

$$\dot{\bar{\bar{C}}}(s,\gamma,\omega,\phi) = \frac{\phi\bar{\bar{C}}(s,\gamma,\omega,0)}{(\phi+\mathcal{M})(\phi-\mathcal{M})} - \frac{\dot{\bar{\bar{F}}}(s,\gamma,\omega,\phi)}{D_z(\phi+\mathcal{M})(\phi-\mathcal{M})}, \tag{B1}$$

where

$$\mathcal{M} = \frac{1}{D_z^{1/2}}\left(s+\gamma^2 D_x + i\gamma U + \omega^2 D_y + \mathcal{A} - \frac{\mathcal{B}}{s+\mathcal{H}}\right)^{1/2}, \tag{B2}$$

(A8)–(A10), and the following property was employed for the Laplace transformation (Roberts and Kaufman, 1966)

$$\dot{\bar{\bar{C}}}(s,\gamma,\omega,\phi) = \int_0^\infty \bar{\bar{C}}(s,\gamma,\omega,z)e^{-\phi z}dz, \tag{B3}$$

where the overdot signifies Laplace transform with respect to space variable z and ϕ is the corresponding the Laplace domain variable.

The Laplace inverse transformation of (B1) with respect to ϕ is

$$\begin{aligned}\bar{\bar{C}}(s,\gamma,\omega,z) = {} & \bar{\bar{C}}(s,\gamma,\omega,0)\left(\frac{e^{-\mathcal{M}z}+e^{\mathcal{M}z}}{2}\right) \\ & + \frac{1}{D_z}\int_0^z \bar{\bar{F}}(s,\gamma,\omega,p)\left(\frac{e^{-\mathcal{M}(z-p)}-e^{\mathcal{M}(z-p)}}{2\mathcal{M}}\right)dp,\end{aligned} \tag{B4}$$

where (A56) and the following Laplace inversion identities were utilized (Roberts and Kaufman, 1966)

$$\mathcal{L}^{-1}\left\{\frac{\phi}{(\phi+\alpha)(\phi+\beta)}\right\} = \frac{\alpha e^{-\alpha z}}{\alpha-\beta} + \frac{\beta e^{-\beta z}}{\beta-\alpha}, \tag{B5}$$

$$\mathcal{L}^{-1}\left\{\frac{1}{(\phi+\alpha)(\phi+\beta)}\right\} = \frac{e^{-\alpha z}-e^{-\beta z}}{\beta-\alpha}. \tag{B6}$$

Applying boundary condition (26) in (B4) and taking the limit $z \to \infty$, $\bar{\bar{\tilde{C}}}(s,\gamma,\omega,0)$ is evaluated to be

$$\bar{\bar{\tilde{C}}}(s,\gamma,\omega,0) = \frac{1}{D_z \mathcal{M}} \int_0^\infty \bar{\bar{\tilde{F}}}(s,\gamma,\omega,p) e^{-\mathcal{M}p}\, dp. \tag{B7}$$

Substituting (B7) into (B4) yields

$$\bar{\bar{\tilde{C}}}(s,\gamma,\omega,z) = \frac{1}{2D_z}\Bigg\{ \int_0^\infty \bar{\bar{\tilde{F}}}(s,\gamma,\omega,p)\Big[\Phi_1(s,\gamma,\omega,z+p) + \Phi_1(s,\gamma,\omega,p-z)\Big]\, dp$$

$$+ \int_0^z \bar{\bar{\tilde{F}}}(s,\gamma,\omega,p)\Big[\Phi_1(s,\gamma,\omega,z-p) - \Phi_1(s,\gamma,\omega,p-z)\Big]\, dp\Bigg\}, \tag{B8}$$

where

$$\Phi_1(s,\gamma,\omega,z) = \frac{e^{-\mathcal{M}z}}{\mathcal{M}}. \tag{B9}$$

Furthermore, for mathematical convenience, let

$$\Phi_1 = \frac{\mathcal{H}\Phi_1}{s+\mathcal{H}} + \frac{s\Phi_1}{s+\mathcal{H}}. \tag{B10}$$

The inverse Laplace transformation of $\Phi_1(s,\gamma,\omega,z)$ with respect to s can be found by employing (A43), where in view of (B9), $\tilde{f}_\circ(s)$ is assumed to be of the following form

$$\tilde{f}_\circ(s) = \frac{\exp\left[-\alpha_1(s+\alpha_2)^{1/2}\right]}{\alpha_3(s+\alpha_2)^{1/2}}, \tag{B11}$$

where α_1, α_2, and α_3 are arbitrary constants. Furthermore, the inverse Laplace transform of $\tilde{f}_\circ(s)$ is (Roberts and Kaufman, 1966, eq. 3.2.16, p. 246)

$$f_\circ(t) = \mathcal{L}^{-1}\left\{\frac{\exp\left[-\alpha_1(s+\alpha_2)^{1/2}\right]}{\alpha_3(s+\alpha_2)^{1/2}}\right\} = \frac{1}{\alpha_3(\pi t)^{1/2}} \exp\left[\frac{-\alpha_1^2}{4t} - \alpha_2 t\right]. \tag{B12}$$

In view of (B9)–(B12), and by following the procedures outlined in Appendix A, the inverse Laplace transform of (B8) with respect to s is given by

$$\bar{\tilde{C}}(t,\gamma,\omega,z) = \frac{1}{2D_z} \int_0^t \int_0^\infty \bar{\tilde{F}}(t-\tau,\gamma,\omega,p)\Bigg[\mathcal{H}\bar{\tilde{\mathcal{P}}}_1(\tau,\gamma,\omega,z+p) + \frac{\partial \bar{\tilde{\mathcal{P}}}_1(\tau,\gamma,\omega,z+p)}{\partial\tau}$$

$$+ \mathcal{H}\bar{\tilde{\mathcal{P}}}_1(\tau,\gamma,\omega,p-z) + \frac{\partial \bar{\tilde{\mathcal{P}}}_1(\tau,\gamma,\omega,p-z)}{\partial\tau}\Bigg]\, dp\, d\tau, \tag{B13}$$

where

$$\bar{\bar{\mathcal{P}}}_1(t,\gamma,\omega,z) = e^{-\mathcal{H}t}\int_0^t I_\circ\Big[2\big(\mathcal{B}\zeta(t-\zeta)\big)^{1/2}\Big]\left(\frac{D_z}{\pi\zeta}\right)^{1/2} \exp\left[-\frac{z^2}{4D_z\zeta} - \Big(\omega^2 D_y + \mathcal{A} - \mathcal{H}\Big)\zeta\right]\mathcal{Q}(\gamma,\zeta)\,d\zeta, \tag{B14}$$

$$\frac{\partial\bar{\bar{\mathcal{P}}}_1(t,\gamma,\omega,z)}{\partial t} = e^{-\mathcal{H}t}\int_0^t\left\{\left(\frac{\mathcal{B}\zeta}{t-\zeta}\right)^{1/2} I_1\Big[2\big(\mathcal{B}\zeta(t-\zeta)\big)^{1/2}\Big] - \mathcal{H}I_\circ\Big[2\big(\mathcal{B}\zeta(t-\zeta)\big)^{1/2}\Big]\right\} \times\left(\frac{D_z}{\pi\zeta}\right)^{1/2}\exp\left[-\frac{z^2}{4D_z\zeta} - \Big(\omega^2 D_y + \mathcal{A} - \mathcal{H}\Big)\zeta\right]\mathcal{Q}(\gamma,\zeta)\,d\zeta + e^{-\mathcal{H}t}\left(\frac{D_z}{\pi t}\right)^{1/2}\exp\left[-\frac{z^2}{4D_z t} - \Big(\omega^2 D_y + \mathcal{A} - \mathcal{H}\Big)t\right]\mathcal{Q}(\gamma,t), \tag{B15}$$

$$\mathcal{Q}(\gamma,t) = \exp\left[-D_x t\left(\gamma^2 + \frac{iU}{D_x}\gamma\right)\right]. \tag{B16}$$

The inverse Fourier transformation of (B13) with respect to γ is

$$\bar{C}(t,x,\omega,z) = \left(\frac{1}{8\pi D_z^2}\right)^{1/2}\int_0^t\int_{-\infty}^{\infty}\int_0^{\infty}\bar{F}(t-\tau,q,\omega,p) \left[\mathcal{H}\bar{\mathcal{P}}_1(\tau,x-q,\omega,z+p) + \frac{\partial\bar{\mathcal{P}}_1(\tau,x-q,\omega,z+p)}{\partial\tau} + \mathcal{H}\bar{\mathcal{P}}_1(\tau,x-q,\omega,p-z) + \frac{\partial\bar{\mathcal{P}}_1(\tau,x-q,\omega,p-z)}{\partial\tau}\right] dp\,dq\,d\tau, \tag{B17}$$

where the definitions of the Fourier inverse transform (A13) and (A14)were employed.

In order to obtain the inverse Fourier transformation of (B14) with respect to γ, only the term $\mathcal{Q}(\gamma,t)$ defined in (B16) requires inversion, and is obtained as follows

$$\mathcal{F}^{-1}\Big\{\mathcal{Q}(\gamma,t)\Big\} = \frac{1}{(2\pi)^{1/2}}\int_{-\infty}^{\infty}\exp\left[-D_x t\left(\gamma^2 + \frac{iU}{D_x}\gamma\right)\right]e^{i\gamma x}\,d\gamma = \left(\frac{1}{2D_x t}\right)^{1/2}\eta(x,t), \tag{B18}$$

where

$$\eta(x,t) = \exp\left[-\frac{1}{D_x}\left(\frac{U^2 t}{4} + \frac{x^2}{4t} - \frac{Ux}{2}\right)\right], \tag{B19}$$

and the latter expression in (B18) is a consequence of employing (A15) and the following integral identities (Gradshteyn and Ryzhik, 1980, eq. 3.923.1 & 2, p. 485)

$$\int_{-\infty}^{\infty} \exp\Big[-\Big(\beta_1\gamma^2 + 2\beta_2\gamma\Big)\Big]\cos(2\beta_3\gamma)\; d\gamma$$

$$= \left(\frac{\pi}{\beta_1}\right)^{1/2} \exp\left[\frac{\beta_1\beta_2^2 - \beta_1\beta_3^2}{\beta_1^2}\right] \cos\left[-\frac{2\beta_1\beta_2\beta_3}{\beta_1^2}\right], \qquad \text{(B20)}$$

$$\int_{-\infty}^{\infty} \exp\Big[-\Big(\beta_1\gamma^2 + 2\beta_2\gamma\Big)\Big]\sin(2\beta_3\gamma)\; d\gamma$$

$$= \left(\frac{\pi}{\beta_1}\right)^{1/2} \exp\left[\frac{\beta_1\beta_2^2 - \beta_1\beta_3^2}{\beta_1^2}\right] \sin\left[-\frac{2\beta_1\beta_2\beta_3}{\beta_1^2}\right], \qquad \text{(B21)}$$

where β_1, β_2, and β_3 are arbitrary constants. Therefore, in view of (B18), the inverse Fourier transformation of (B14) is

$$\bar{\mathcal{P}}_1(t,x,\omega,z) = e^{-\mathcal{H}t} \int_0^t I_\circ\Big[2\big(\mathcal{B}\zeta(t-\zeta)\big)^{1/2}\Big] \left(\frac{D_z}{2\pi D_x\zeta^2}\right)^{1/2}$$

$$\times \exp\left[-\frac{z^2}{4D_z\zeta} - \Big(\omega^2 D_y + \mathcal{A} - \mathcal{H}\Big)\zeta\right] \eta(x,\zeta)\; d\zeta. \qquad \text{(B22)}$$

The inverse Fourier transformation of (B17) with respect to ω is

$$C(t,x,y,z) = \frac{1}{4\pi D_z} \int_0^t \int_{-\infty}^{\infty} \int_{-\infty}^{\infty} \int_0^{\infty} F(t-\tau,q,v,p)$$

$$\times \left[\mathcal{H}\mathcal{P}_1(\tau,x-q,y-v,z+p) + \frac{\partial\mathcal{P}_1(\tau,x-q,y-v,z+p)}{\partial\tau}\right.$$

$$\left. + \mathcal{H}\mathcal{P}_1(\tau,x-q,y-v,p-z) + \frac{\partial\mathcal{P}_1(\tau,x-q,y-v,p-z)}{\partial\tau}\right] dpdvdqd\tau. \qquad \text{(B23)}$$

In view of the following inverse Fourier transform relationship (Kreryszig, 1993, eq. 9, p. 621)

$$\mathcal{F}^{-1}\left\{\exp\Big[-\omega^2 D_y\zeta\Big]\right\} = \left(\frac{1}{2D_y\zeta}\right)^{1/2} \exp\left[-\frac{y^2}{4D_y\zeta}\right], \qquad \text{(B24)}$$

the inverse Fourier transformation of (B22) is

$$\mathcal{P}_1(t,x,y,z) = e^{-\mathcal{H}t}\int_0^t I_\circ\Big[2\big(\mathcal{B}\zeta(t-\zeta)\big)^{1/2}\Big]\left(\frac{D_z}{4\pi D_x D_y \zeta^3}\right)^{1/2} \times \exp\left[-\frac{z^2}{4D_z\zeta} - \frac{y^2}{4D_y\zeta} - \big(\mathcal{A}-\mathcal{H}\big)\zeta\right]\eta(x,\zeta)\,d\zeta. \tag{B25}$$

Furthermore, in order to complete the description of (B23), the derivative of $\mathcal{P}_1(t,x,y,z)$ with respect to t is obtained as follows

$$\begin{aligned}\frac{\partial\mathcal{P}_1(t,x,y,z)}{\partial t} = e^{-\mathcal{H}t}\int_0^t \left\{\left(\frac{\mathcal{B}\zeta}{t-\zeta}\right)^{1/2} I_1\Big[2\big(\mathcal{B}\zeta(t-\zeta)\big)^{1/2}\Big] - \mathcal{H}I_\circ\Big[2\big(\mathcal{B}\zeta(t-\zeta)\big)^{1/2}\Big]\right\} \\ \times\left(\frac{D_z}{4\pi D_x D_y\zeta^3}\right)^{1/2}\exp\left[-\frac{z^2}{4D_z\zeta} - \frac{y^2}{4D_y\zeta} - \big(\mathcal{A}-\mathcal{H}\big)\zeta\right]\eta(x,\zeta)\,d\zeta \\ + e^{-\mathcal{H}t}\left(\frac{D_z}{4\pi D_x D_y t^3}\right)^{1/2}\exp\left[-\frac{z^2}{4D_z t} - \frac{y^2}{4D_y t} - \big(\mathcal{A}-\mathcal{H}\big)t\right]\eta(x,t).\end{aligned} \tag{B26}$$

Substituting (B19) into (B25) and (B26) and subsequently substituting the resulting expressions into (B23) yields the desired generalized analytical solution (27) and (28).

Derivation of the Analytical Solution for an Aquifer with Finite Thickness

The analytical solution for the case of an aquifer with finite thickness is obtained by solving (4) subject to (8)–(10), (25), and (39). Taking Laplace transform with respect to time variable t, Fourier transforms with respect to space variables x and y, and finite Fourier cosine transform with respect to space variable z of (4) and subsequently employing transformed initial condition (8) yields

$$\ddot{\hat{\bar{C}}}(s,\gamma,\omega,\psi_m) = \frac{\ddot{\hat{\bar{F}}}(s,\gamma,\omega,\psi_m)}{\gamma^2 D_x + i\gamma U + \mathcal{E}}, \tag{C1}$$

where

$$\mathcal{E} = \omega^2 D_y + \psi_m^2 D_z + \mathcal{A} + s - \frac{\mathcal{B}}{s+\mathcal{H}}, \tag{C2}$$

the Laplace and Fourier transformation properties (A8)–(A10), and the following finite Fourier cosine transformation and operational property were employed (Churchill, 1958, p. 294)

$$\ddot{\hat{\bar{C}}}(s,\gamma,\omega,\psi_m) = \int_0^H \hat{\bar{C}}(s,\gamma,\omega,z)\cos(\psi_m z)dz, \tag{C3}$$

$$\mathcal{F}_{\text{fc}}\left\{\frac{d^2 f_3(z)}{dz^2}\right\} = \psi_m^2 \ddot{f}_3(\psi_m^2) - \frac{df_3(0)}{dz} + (-1)^m \frac{df_3(H)}{dz}, \qquad (m = 0,1,2...) \tag{C4}$$

where the double over–dot signifies finite Fourier cosine transform with respect to space variable z with corresponding finite Fourier cosine transform variable $\psi_m = m\pi/H$; $\mathcal{F}_{\text{fc}}$ is the finite Fourier cosine transform operator; and f_3 is an arbitrary function.

The Fourier inverse transformation of (C1) with respect to γ is

$$\ddot{\bar{C}}(s,x,\omega,\psi_m) = \frac{\ddot{\hat{\bar{F}}}(s,x,\omega,\psi_m)}{2\pi D_x} * \left(\int_{-\infty}^{\infty} \frac{\cos\gamma x}{\gamma^2 + \frac{i\gamma U}{D_x} + \frac{\mathcal{E}}{D_x}}\, d\gamma + \int_{-\infty}^{\infty} \frac{i\sin\gamma x}{\gamma^2 + \frac{i\gamma U}{D_x} + \frac{\mathcal{E}}{D_x}}\, d\gamma \right), \tag{C5}$$

where the definitions of the Fourier inverse transform (A13) and (A14) and Euler's formula (A15) were employed.

In view of the integral identities (A16) and (A17), (C2), and application of the convolution theorem, (C5) is simplified as

$$\tilde{\tilde{C}}(s,x,\omega,\psi_m) = \int_{-\infty}^{\infty} \tilde{\tilde{F}}(s,q,\omega,\psi_m)\ \Psi_1(s,x-q,\omega,\psi_m)\ dq, \tag{C6}$$

where

$$\Psi_1(s,x,\omega,\psi_m) = \left(\frac{1}{4D_xD_y\left(\omega^2+\mathcal{S}_1\right)}\right)^{1/2} \exp\left[\frac{Ux}{2D_x}\right] \exp\left[-x\left(\left(\omega^2+\mathcal{S}_1\right)\frac{D_y}{D_x}\right)^{1/2}\right], \tag{C7}$$

$$\mathcal{S}_1 = \frac{1}{D_y}\left(\psi_m^2 D_z + \mathcal{A} + s - \frac{\mathcal{B}}{s+\mathcal{H}} + \frac{U^2}{4D_x}\right). \tag{C8}$$

In view of (A13), (A14), and (C7), the inverse Fourier transformation of (C6) with respect to ω is given by

$$\tilde{\tilde{C}}(s,x,y,\psi_m) = \left(\frac{1}{16\pi^2 D_xD_y}\right)^{1/2} \int_{-\infty}^{\infty} \exp\left[\frac{U(x-q)}{2D_x}\right]$$
$$\times \left\{\tilde{\tilde{F}}(s,q,y,\psi_m) * \left[\int_{-\infty}^{\infty} \Theta\cos(\omega y)d\omega + \int_{-\infty}^{\infty} i\Theta\sin(\omega y)d\omega\right]\right\} dq, \tag{C9}$$

where

$$\Theta = \left(\frac{1}{\omega^2+\mathcal{S}_1}\right)^{1/2} \exp\left[-(x-q)\left(\left(\omega^2+\mathcal{S}_1\right)\frac{D_y}{D_x}\right)^{1/2}\right], \tag{C10}$$

and Euler's formula (A15) was employed for the derivation of (C9). It should be noted that Θ as well as $\cos(\omega y)$ are even functions of ω, whereas $\sin(\omega y)$ is an odd function of ω. Therefore, the trigonometric integrals are evaluated by employing the similar procedures as shown by (A26)–(A28).

In view of (A26), (A27), and application of the convolution theorem, (C9) reduces to

$$\tilde{\tilde{C}}(s,x,y,\psi_m) = \int_{-\infty}^{\infty}\int_{-\infty}^{\infty} \tilde{\tilde{F}}(s,q,v,\psi_m)\ g_\circ(s,x-q,y-v,\psi_m)\ dv\ dq, \tag{C11}$$

where

$$g_\circ(s,x,y,\psi_m) = \left(\frac{1}{4\pi^2 D_xD_y}\right)^{1/2} \exp\left[\frac{Ux}{2D_x}\right] K_\circ\left[\mathcal{S}_1^{1/2}\left(y^2 + x^2\frac{D_y}{D_x}\right)^{1/2}\right]. \tag{C12}$$

In view of (C8) and (C12), the inverse Laplace transformation of (C11) with respect to s is given by

$$\ddot{C}(t,x,y,\psi_m) = \left(\frac{1}{4\pi^2 D_x D_y}\right)^{1/2} \int_{-\infty}^{\infty}\int_{-\infty}^{\infty} \exp\left[\frac{U(x-q)}{2D_x}\right] \times \left[\ddot{F}(t,q,v,\psi_m) * \mathcal{L}^{-1}\left\{K_o\Big[\mathcal{M}_1(s,x-q,y-v,\psi_m)\Big]\right\}\right] dv\, dq, \tag{C13}$$

where

$$\mathcal{M}_1 = \mathcal{M}_2\left(s - \frac{\mathcal{B}}{s+\mathcal{H}} + \mathcal{M}_3\right)^{1/2}, \tag{C14}$$

$$\mathcal{M}_2 = \left[\frac{(x-q)^2}{D_x} + \frac{(y-v)^2}{D_y}\right]^{1/2}, \tag{C15}$$

$$\mathcal{M}_3 = \psi_m^2 D_z + \frac{U^2}{4D_x} + \mathcal{A}. \tag{C16}$$

For mathematical convenience, let

$$K_o[\mathcal{M}_1] = \frac{\mathcal{H}K_o[\mathcal{M}_1]}{s+\mathcal{H}} + \frac{sK_o[\mathcal{M}_1]}{s+\mathcal{H}}. \tag{C17}$$

The inverse Laplace transformation of $K_o\Big[\mathcal{M}_1(s,x-q,y-v,\psi_m)\Big]$ with respect to s can be found by employing (A43), where, in view of (C14), $\widetilde{f}_o(s)$ is assumed to be of the following form

$$\widetilde{f}_o(s) = K_o\left[\beta_1\Big(s+\beta_2\Big)^{1/2}\right]. \tag{C18}$$

The inverse Laplace transform of $\widetilde{f}_o(s)$ is given by (Roberts and Kaufman, 1966, eq. 3, p. 169 & eq. 13.2.1, p. 304)

$$f_o(t) = \mathcal{L}^{-1}\left\{K_o\left[\beta_1\Big(s+\beta_2\Big)^{1/2}\right]\right\} = \frac{1}{2t}\exp\left[\frac{-\beta_1^2}{4t} - \beta_2 t\right]. \tag{C19}$$

In view of (C14)–(C19), and by following the procedures outlined in Appendix A, the inverse Laplace transformation of (C13) with respect to s is as follows

$$\ddot{C}(t,x,y,\psi_m) = \left(\frac{1}{16\pi^2 D_x D_y}\right)^{1/2} \int_0^t \int_{-\infty}^{\infty}\int_{-\infty}^{\infty} \exp\left[\frac{U(x-q)}{2D_x}\right] e^{-\mathcal{H}\tau}\, \ddot{F}(t-\tau,q,v,\psi_m)$$

$$\times \left\{ \int_0^{\tau} \left(\frac{\mathcal{B}}{\zeta(\tau-\zeta)} \right)^{1/2} I_1\left[2\left(\mathcal{B}\zeta(\tau-\zeta)\right)^{1/2} \right] \right.$$
$$\exp\left[-\zeta\left(\psi_m^2 D_z + \mathcal{A} + \frac{U^2}{4D_x} - \mathcal{H} \right) \right]$$
$$\times \exp\left[-\frac{1}{4\zeta}\left(\frac{(x-q)^2}{D_x} + \frac{(y-v)^2}{D_y} \right) \right] d\zeta$$
$$+ \frac{1}{\tau} \exp\left[-\tau\left(\psi_m^2 D_z + \mathcal{A} + \frac{U^2}{4D_x} - \mathcal{H} \right) \right]$$
$$\left. \times \exp\left[-\frac{1}{4\tau}\left(\frac{(x-q)^2}{D_x} + \frac{(y-v)^2}{D_y} \right) \right] \right\} dv\ dq\ d\tau. \qquad \text{(C20)}$$

The inverse Fourier cosine transformation of (C20) with respect to ψ_m is given by

$$C(t,x,y,z) = \left(\frac{1}{16\pi^2 D_x D_y} \right)^{1/2} \int_0^t \int_{-\infty}^{\infty} \int_{-\infty}^{\infty} \exp\left[\frac{U(x-q)}{2D_x} \right] e^{-\mathcal{H}\tau}$$
$$\times \left\{ \int_0^{\tau} \left(\frac{\mathcal{B}}{\zeta(\tau-\zeta)} \right)^{1/2} I_1\left[2\left(\mathcal{B}\zeta(\tau-\zeta)\right)^{1/2} \right] \exp\left[-\frac{1}{4\zeta}\left(\frac{(x-q)^2}{D_x} + \frac{(y-v)^2}{D_y} \right) \right] \right.$$
$$\times \exp\left[-\zeta\left(\mathcal{A} + \frac{U^2}{4D_x} - \mathcal{H} \right) \right] \mathcal{F}_{\text{fc}}^{-1}\left\{ \ddot{F}(t-\tau,q,v,\psi_m) \exp\left[-\psi_m^2 D_z \zeta \right] \right\} d\zeta$$
$$+ \frac{1}{\tau} \exp\left[-\frac{1}{4\tau}\left(\frac{(x-q)^2}{D_x} + \frac{(y-v)^2}{D_y} \right) \right] \exp\left[-\tau\left(\mathcal{A} + \frac{U^2}{4D_x} - \mathcal{H} \right) \right]$$
$$\left. \times \mathcal{F}_{\text{fc}}^{-1}\left\{ \ddot{\bar{F}}(t-\tau,q,v,\psi_m) \exp\left[-\psi_m^2 D_z \tau \right] \right\} \right\} dv\ dq\ d\tau, \qquad \text{(C21)}$$

where $\mathcal{F}_{\text{fc}}^{-1}$ is the inverse finite Fourier cosine operator defined as

$$\mathcal{F}_{\text{fc}}^{-1}\left\{ \ddot{f}_3(\psi_m) \right\} = \frac{\ddot{f}_3(0)}{H} + \frac{2}{H} \sum_{m=1}^{\infty} \ddot{f}_3(\psi_m) \cos(\psi_m z), \qquad 0 \le z \le H. \qquad \text{(C22)}$$

In view of (C22), (C21) is simplified to the form of the generalized analytical solution (40)–(42).

Abramowitz, M. and I. A. Stegun. 1972. *Handbook of Mathematical Functions*, 1046 pp., Dover.

Bales, R. C., S. R. Hinkle, T. W. Kroeger, and K. Stocking. 1991. Bacteriophage adsorption during transport through porous media: Chemical perturbations and reversibility, *Env. Sci. and Tech.*, *25*(12), 2088–2095.

Batu, V. 1989. A generalized two–dimensional analytical solution for hydrodynamic dispersion in bounded media with the first–type boundary condition at the source, *Water Resour. Res.*, *25*(6), 1125–1132.

Batu, V. 1993. A generalized two–dimensional analytical solute transport model in bounded media for flux–type finite multiple sources, *Water Resour. Res.*, *29*(8) 1125–1132.

Batu, V. and M. T. van Genuchten. 1990. First– and third–type boundary conditions in two–dimensional solute transport modeling, *Water Resour. Res.*, *26*(2), 339–350.

Bellin, A., A. Rinaldo, W. J. P. Bosma, S. E. A. T. M. van der Zee, and Y. Rubin. 1993. Linear equilibrium adsorbing solute transport in physically and chemically heterogeneous porous formations, 1, Analytical solutions, *Water Resour. Res.*, *29*(12), 4019–4030.

Bitton, G., C. P. Gerba. 1984. *Groundwater Pollution Microbiology*, Wiley, New York.

Blanc, R., A. Nasser. 1996. Effect of effluent quality and temperature on the persistence of viruses in soil, *Wat. Sci. Tech.*, *33*(10–11), 237–242.

Chrysikopoulos, C. V. 1995. Three–dimensional analytical models of contaminant transport from nonaqueous phase liquid pool dissolution in saturated subsurface formations, *Water Resour. Res.*, *31*(4), 1137–1145.

Chrysikopoulos, C. V. and Y. Sim. 1996. One–dimensional virus transport in homogeneous porous media with time dependent distribution coefficient, *J. Hydrol.*, *185*, 199–219.

Chrysikopoulos, C. V., E. A. Voudrias, and M. M. Fyrillas. 1994. Modeling of contaminant transport resulting from dissolution of nonaqueous phase liquid pools in saturated porous media, *Trans. Porous Media*, *16*(2), 125–145.

Churchill, R. V. 1958. *Operational Mathematics*, McGraw-Hill, New York.

Crane, S. R., and J. A. Moore. 1986. Modeling enteric bacterial die–off: A review, *Water, Air, Soil Pollut.*, *27*, 411–439.

Davis, M. L. and D. A. Cornwell. 1991. *Introduction to Environmental Engineering*, McGraw–Hill.

Gerba, C. P. 1984. Applied and theoretical aspects of virus adsorption to surfaces, *Adv. Appl. Microb.*, *30*, 133–168.

Goltz, M. N. and P. V. Roberts. 1986. Three–dimensional solutions for solute transport in an infinite medium with mobile and immobile zones, *Water Resour. Res., 22*(7), 1139–1148.

Gradshteyn, I. S. and I. M. Ryzhik. 1980. *Table of Integral, Series, and Products*, Academic Press.

Grant, S. B., E. J. List, and M. E. Lidstrom. 1993. Kinetic analysis of virus Adsorption and inactivation in batch experiments; virus adsorption, virus inactivation, equilibrium isotherms, *Water Resour. Res., 29*(7), 2067–2085.

Greenberg, M. D. 1978. *Foundations of Applied Mathematics*, Prentice Hall, N. J.

Grosser, P. W. 1984. A one-dimensional mathematical model of virus transport, Paper presented at the *Second International Conference on Ground-Water Quality Research*, Tulsa, OK., Mar. 26–29.

Gupta, A. and M. Chaudhuri. 1995. Enteric virus removal/inactivation by coal–based media, *Wat. Res., 29*(2), 511–516.

Haridas, A. 1984. *A Mathematical Model of Microbial Transport in Porous Media*, Ph.D. Dissertation, University of Delaware.

Hassani, S. 1991. *Foundations of Mathematical Physics*, Allyn and Bacon, Boston.

Huber, M. S., C. P. Gerba, and M. Abbaszadegan. 1994. Study of persistence of enteric viruses in landfilled disposable diapers, *Environ. Sci. Technol., 28*, 1767–1772.

Hunt, B. 1978. Dispersive Sources in uniform groundwater flow, *J. Hydraul. Div. Am. Soc. Civ. Eng., 104*(HY1), 75–85.

Hurst, C. J., C. P. Gerba, and I. Cech. 1980. Effects of Environmental variables and soil characteristics on virus survival in soil, *Appl. Environ. Microb., 40*(6), 1067–1079.

Hurst, C. J., C. P. Gerba, J. C. Lance, and R. C. Rice. 1980. Survival of enteroviruses in rapid–infiltration basins during the land application of wastewater, *App. Environ. Microb., 40*(2), 192–200.

IMSL. 1991. *IMSL MATH/LIBRARY user's manual*, ver. 2.0, IMSL, Houston.

Kahaner, D., C. Moler, and S. Nash. 1989. *Numerical Methods and Software*, Prentice Hall, N. J.

Knopman, D. S., and C. I. Voss. 1987. Behavior of sensitivities in the one–dimensional advection–dispersion equation; Implications for parameter estimation and sampling data, *Water Resour. Res., 23*(2), 253–272.

Koda, M., A. H. Dogru, and J. H. Seinfeld. 1979 Sensitivity analysis of partial differential equations with application to reaction and diffusion processes, *J. Comp. Physics, 30*, 259–282.

Kreyszig, E. 1993. *Advanced Engineering Mathematics*, 7th ed., Wiley, New York.

Lapidus, L. and N. R. Amundson. 1952. Mathematics of adsorption in beds, VI. The effect of longitudinal diffusion in ion exchange and chromatographic columns, *J. Phys. Chem.*, *56*, 984–988.

Leij, F. J. and J. H. Dane. 1990. Analytical solutions of the one–dimensional advection equation and two– or three–dimensional dispersion equation, *Water Resour. Res.*, *26*(7), 1475–1482.

Leij, F. J., T. H. Skaggs, and M. Th. van Genuchten. 1991. Analytical solutions for solute transport in three–dimensional semi–infinite porous media, *Water Resour. Res.*, *27*(10), 2719–2733.

Leij, F. J., N. Toride, and M. Th. van Genuchten. 1993. Analytical solutions for nonequilibrium solute transport in three–dimensional porous media, *J. Hydrol.*, *151*, 193–228.

Matthess, G., A. Pekdeger, and J. Schroeter. 1988. Persistence and transport of bacteria and viruses in groundwater: A conceptual evaluation, *J. Contamin. Hydrol.*, *2*, 171–188.

Metcalf and Eddy. 1991. *Wastewater Engineering: Collection, Treatment, Disposal*, Metcalf & Eddy, Inc., McGraw-Hill, New York.

Park, N., T. N. Blanford, and P. S. Huyakorn. 1992. VIRALT: A modular semi–analytical and numerical model for simulating viral transport in ground water, International Ground Water Modeling Center, Colorado School of Mines, Golden, CO.

Parkinson, J. S., and and R. J. Huskey. 1971. Deletion Mutants of Bacteriophage Lambda, 1, Isolation and initial characterization, *J. Mol. Biol.*, *56*, 369–384.

Pollard, E. C., and W. Solosko. 1971. The thermal inactivation of T_4 and λ Bacteriophage, *Biophys. J.*, *11*, 66–74.

Powelson, D. K., C. P. Gerba, and M. T. Yahya. 1993. Virus transport and removal in wastewater during aquifer recharge, *Water Res.*, *27*(4), 583–590.

Reddy, K. R., R. Khaleel, and M. R. Overcash. 1981. Behavior and transport of microbial pathogens and indicator organisms in soils treated with organic wastes, *J. Environ. Qual.*, *10*(3), 255–266.

Roberts, G. E. and H. Kaufman. 1966. *Table of Laplace Transforms*, W. B. Saunders, Philadelphia, PA.

Sim, Y. and C. V. Chrysikopoulos. 1995. Analytical models for one–dimensional virus transport in saturated porous media, *Water Resour. Res.*, *31*(5), 1429–1437. (Correction, *Water Resour. Res.*, *32*(5), 1473, 1996)

Sim, Y. and C. V. Chrysikopoulos. 1966. One–dimensional virus transport in porous media with time dependent inactivation rate coefficients, *Water Resour. Res.*, *32*(8), 2607–2611.

Teutsch, G., K. Herbold–Paschke, D. Tougianidou, T. Hahn, and K. Botzenhart. 1991. Transport of microorganisms in the underground–Processes, experiments, and simulation models, *Wat. Sci. Tech. 24*(2), 309–314.

Tim, U. S. and S. Mostaghimi. 1991. Model for predicting virus movement through soils. *Ground Water, 29*(2), 251–259.

van Dujin, C. J. and S. E. A. T. M. van der Zee. 1986. Solute transport parallel to an separating two different porous materials, *Water Resour. Res., 22*(13), 1779–1789.

van Kooten, J. J. A. 1996. A method to solve the advection–dispersion equation with a kinetic adsorption isotherm, *Adv. Water Resour., 19*(4), 193–206.

Vilker, V. L., L. H. Frommhagen, R. Kamda, and S. Sundaram. 1978. Application of ion exchange/adsorption models to virus transport in percolating beds, *AIChE Symp. Ser., 74*(178), 84–92.

Vilker, V. L., and W. D. Burge. 1980. Adsorption Mass Transfer model for virus transfer in soils, *Water Research, 14*, 783–790.

Vilker, V. L. 1981. Simulating virus movement in soils, in *Modeling Waste Renovation: Land Treatment*, edited by I. K. Iskandar, pp. 223–253, John Wiley and Sons.

Yahya, M. T., L. Galsomies, C. P. Gerba, and R. C. Bales. 1993. Survival of bacteriophages MS–2 and PRD–1 in ground water, *Wat. Sci. Tech., 27*(3–4), 409–412.

Yamagishi, H., and H. Ozeki. 1972. Comparative study of thermal inactivation of phage $\phi 80$ and Lambda, *Virology, 48*, 316–322.

Yates, M. V., and S. R. Yates. 1988. Modeling microbial fate in the subsurface environment, *Crit. Rev. Environ. Control, 17*(4), 307–344.

Yates, M. V. and Y. Ouyang. 1992. VIRTUS, a model of virus transport in unsaturated soils, *Appl. Environ. Microb., 58*(5), 1609–1616.